



HAL
open science

The coupled ^{182}W - ^{142}Nd record of early terrestrial mantle differentiation

Igor Puchtel, Janne Blichert-Toft, Mathieu Touboul, Mary Horan, Mary Walker

► **To cite this version:**

Igor Puchtel, Janne Blichert-Toft, Mathieu Touboul, Mary Horan, Mary Walker. The coupled ^{182}W - ^{142}Nd record of early terrestrial mantle differentiation. *Geochemistry, Geophysics, Geosystems*, 2016, 17 (6), pp.2168-2193. 10.1002/2016GC006324 . hal-02110085

HAL Id: hal-02110085

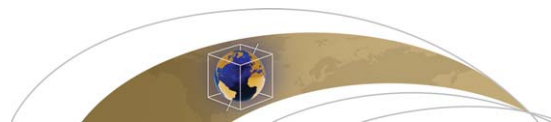
<https://hal.science/hal-02110085>

Submitted on 7 Jan 2022

HAL is a multi-disciplinary open access archive for the deposit and dissemination of scientific research documents, whether they are published or not. The documents may come from teaching and research institutions in France or abroad, or from public or private research centers.

L'archive ouverte pluridisciplinaire **HAL**, est destinée au dépôt et à la diffusion de documents scientifiques de niveau recherche, publiés ou non, émanant des établissements d'enseignement et de recherche français ou étrangers, des laboratoires publics ou privés.

Copyright



RESEARCH ARTICLE

10.1002/2016GC006324

The coupled ^{182}W - ^{142}Nd record of early terrestrial mantle differentiationIgor S. Puchtel¹, Janne Blichert-Toft², Mathieu Touboul^{1,2}, Mary F. Horan³, and Richard J. Walker¹

Key Points:

- Komatiites from the 3.55 Ga Schapenburg Greenstone Remnant in South Africa show coupled depletions in ^{142}Nd and ^{182}W
- The komatiites were derived from a mantle domain that formed within the first 30 Ma of Solar System history
- The products of early terrestrial differentiation survived planetary accretion and mantle mixing for 1.0 Ga

Correspondence to:

I. S. Puchtel,
ipuchtel@umd.edu

Citation:

Puchtel, I. S., J. Blichert-Toft, M. Touboul, M. F. Horan, and R. J. Walker (2016), The coupled ^{182}W - ^{142}Nd record of early terrestrial mantle differentiation, *Geochem. Geophys. Geosyst.*, 17, 2168–2193, doi:10.1002/2016GC006324.

Received 25 FEB 2016

Accepted 12 MAY 2016

Accepted article online 18 MAY 2016

Published online 18 JUN 2016

¹Department of Geology, University of Maryland, College Park, Maryland, USA, ²Laboratoire de Géologie de Lyon, Ecole Normale Supérieure de Lyon, Université Claude Bernard Lyon 1, CNRS UMR 5276, Lyon, France, ³Department of Terrestrial Magnetism, Carnegie Institution of Science, Washington, District of Columbia, USA

Abstract New Sm-Nd, Lu-Hf, Hf-W, and Re-Os isotope data, in combination with highly siderophile element (HSE, including Re, Os, Ir, Ru, Pt, and Pd) and W abundances, are reported for the 3.55 Ga Schapenburg komatiites, South Africa. The Schapenburg komatiites define a Re-Os isochron with an age of 3550 ± 87 Ma and initial $\gamma^{187}\text{Os} = +3.7 \pm 0.2$ (2SD). The absolute HSE abundances in the mantle source of the Schapenburg komatiite system are estimated to be only $29 \pm 5\%$ of those in the present-day bulk silicate Earth (BSE). The komatiites were derived from mantle enriched in the decay products of the long-lived ^{147}Sm and ^{176}Lu nuclides (initial $\epsilon^{143}\text{Nd} = +2.4 \pm 0.1$, $\epsilon^{176}\text{Hf} = +5.7 \pm 0.3$, 2SD). By contrast, the komatiites are depleted, relative to the modern mantle, in ^{142}Nd and ^{182}W ($\mu^{182}\text{W} = -8.4 \pm 4.5$, $\mu^{142}\text{Nd} = -4.9 \pm 2.8$, 2SD). These results constitute the first observation in terrestrial rocks of coupled depletions in ^{142}Nd and ^{182}W . Such isotopic depletions require derivation of the komatiites from a mantle domain that formed within the first ~ 30 Ma of Solar System history and was initially geochemically enriched in highly incompatible trace elements as a result of crystal-liquid fractionation in an early magma ocean. This mantle domain further must have experienced subsequent melt depletion, after ^{182}Hf had gone extinct, to account for the observed initial excesses in ^{143}Nd and ^{176}Hf . The survival of early-formed ^{182}W and ^{142}Nd anomalies in the mantle until at least 3.55 Ga indicates that the products of early planetary differentiation survived both later planetary accretion and convective mantle mixing during the Hadean. This work moreover renders unlikely that variable late accretion, by itself, can account for all of the observed W isotope variations in Archean rocks.

1. Introduction

The ^{182}Hf - ^{182}W isotopic system ($t_{1/2} = 8.9$ Ma) has been widely applied to constrain the timing of metal-silicate segregation in cosmochemical materials, including iron meteorites [Kleine *et al.*, 2004a, 2004b, 2009]. The utility of the Hf-W chronometer stems from the fact that Hf is a strongly lithophile trace element, while W is moderately siderophile. In addition, both elements are highly refractory. Thus, Hf is efficiently fractionated from W by metal-silicate equilibration, such as occurs during planetary core segregation. In addition to cosmochemical applications, several recent studies have documented enrichments of ^{182}W , relative to the modern mantle, in terrestrial rocks formed during the first half of Earth history [Willbold *et al.*, 2011, 2015; Touboul *et al.*, 2012, 2014; Rizo *et al.*, 2016]. These isotopic enrichments have been interpreted within the framework of two broad categories of primordial processes. The first is disproportional late accretion [Willbold *et al.*, 2011, 2015; Kruijer *et al.*, 2015; Touboul *et al.*, 2015]. Late accretion is a process commonly proposed to account for relatively high absolute, and chondritic relative, abundances of highly siderophile elements (HSE; Re, Os, Ir, Ru, Pt, Rh, Pd, and Au) in the present-day mantle. It requires addition to the mantle of ~ 0.5 wt.% of Earth's mass of HSE-rich planetesimals with chondritic bulk compositions after core formation was complete [Kimura *et al.*, 1974; Morgan *et al.*, 1981; Chou *et al.*, 1983]. Chondrites have ~ 20 times higher W abundances and ~ 200 ppm less radiogenic $^{182}\text{W}/^{184}\text{W}$ ratios than the modern terrestrial mantle; as a result, late accretion would drive the $^{182}\text{W}/^{184}\text{W}$ ratio of the mantle to a composition 20–30 ppm less radiogenic than the pre late accretionary mantle [Willbold *et al.*, 2011]. Thus, mantle, to which little or no late accretionary component was added, would be ^{182}W -enriched, compared with mantle to which a full complement of late accretionary component was added. A corollary of this model is that such a mantle source would also be depleted in the HSE, compared to the modern mantle.

A second category of processes capable of generating ^{182}W heterogeneity in the mantle is metal-silicate or silicate-silicate fractionation operating within the first ~ 50 Ma of Solar System history while ^{182}Hf was extant [e.g., Touboul *et al.*, 2012]. Metal-silicate equilibration, followed by removal of the metal from an isolated mantle domain, such as a basal magma ocean, would leave a silicate domain with high Hf/W, due to the extraction of most of the W into the metal. Alternatively, crystal-liquid fractionation in a purely silicate system, such as a global magma ocean, would lead to high Hf/W in early-formed cumulates and low Hf/W in the residual liquid due to the more incompatible nature of W compared with Hf. If any of these fractionation processes occurred while ^{182}Hf was extant, excesses in ^{182}W would eventually be created in both the silicates left after metal segregation and the silicate cumulates in the differentiated primordial magma ocean, whereas the complementary residual magma ocean liquid would evolve into deficits in ^{182}W , compared to the ambient mantle.

To further constrain the processes involved in the generation of ^{182}W isotopic anomalies in the Earth's mantle, we determined the $^{182}\text{W}/^{184}\text{W}$, $^{142,143}\text{Nd}/^{144}\text{Nd}$, $^{176}\text{Hf}/^{177}\text{Hf}$, and $^{187}\text{Os}/^{188}\text{Os}$ compositions and HSE abundances of 3.55 Ga komatiites from the Schapenburg Greenstone Remnant (SGR) of the Barberton Greenstone Belt (BGB) in South Africa using a newly obtained set of drill core samples. Previously, based on a set of surface outcrop samples from the study of Lécuyer *et al.* [1994], the Schapenburg komatiites were found to have initial $^{187}\text{Os}/^{188}\text{Os}$ enriched by $3.7 \pm 0.3\%$ relative to the chondritic reference at that time [Puchtel *et al.*, 2009], indicating their derivation from a mantle source with long-term, suprachondritic Re/Os. Evidence for long-term suprachondritic Re/Os in precursor mantle also was reported for the 2.8 Ga Kostomuksha komatiites [Puchtel *et al.*, 2005; Touboul *et al.*, 2012], and in that case, moreover, the ^{187}Os excesses were accompanied by a corresponding excess in ^{182}W of ~ 15 ppm. The coupled ^{187}Os - ^{182}W enrichments in the Kostomuksha komatiites led Touboul *et al.* [2012] to conclude that these isotopic compositions were caused by fractionation of Re/Os and Hf/W in a magma ocean. Thus, the Schapenburg komatiites provide an important complement to the Kostomuksha komatiites with regard to whether ^{187}Os and ^{182}W enrichments in the mantle sources of komatiites can be linked, and whether the process at work spans the entire Hadean and Archean eras. In addition, the Schapenburg komatiites are characterized by the lowest known projected abundances of HSE in their mantle source, compared to other well-studied early Archean komatiites. Puchtel *et al.* [2009] estimated absolute HSE abundances of $\sim 25\%$ of bulk silicate Earth (BSE) estimates, as well as fractionated relative abundances, in the source of the Schapenburg komatiites. If the low HSE abundances reflect a deficiency in late accretionary components, as suggested by Maier *et al.* [2009] for some early Archean komatiites, the Schapenburg komatiites would be expected to have ^{182}W excesses of ~ 10 – 21 ppm. As will be shown here, we instead find the combination of low HSE abundances and ^{182}W deficits, which present a new challenge to the model proposed by Maier *et al.* [2009].

2. Geological Background, Samples, and Previous Studies

The geology of the SGR is described in detail in Anhaeusser [1983, 1991], and brief accounts of petrological, geochemical, and isotopic features of the SGR komatiites are given in Lécuyer *et al.* [1994], Blichert-Toft *et al.* [2004], and Puchtel *et al.* [2009]. The SGR is a 12×2.5 km sliver of alternating volcanic and sedimentary units that belongs to a trail of greenstone fragments within the tonalite-trondhjemite gneisses surrounding the BGB [Anhaeusser and Robb, 1980]; the greenstone lithologies of the fragments were proposed to be equivalents to the two lowermost formations of the Onverwacht Group of the BGB, i.e., the Sandspruit and Theespruit Formations [Viljoen and Viljoen, 1969].

The volcano-sedimentary sequences of the SGR are cyclic in nature. Each cycle consists of komatiitic lavas at the base overlain by komatiitic basalts, which in turn are capped by banded iron formations. All rocks have undergone pervasive seafloor alteration and greenschist to amphibolite facies metamorphism, which resulted in nearly complete obliteration of all magmatic mineral assemblages. Within the sampling locality, komatiites form a series of differentiated lava flows that vary in thickness from ~ 20 cm to ~ 1.5 m and have a classic differentiated structure [Pyke *et al.*, 1973] consisting of a lower cumulate, or B-zone, and an upper spinifex, or A-zone. Samples examined in previous studies came from surface outcrops of two single differentiated komatiite lava flows, the 1.1 m thick Carl's flow and the 0.85 m thick Patricia's flow [Lécuyer *et al.*, 1994; Blichert-Toft *et al.*, 2004; Puchtel *et al.*, 2009]. For the present study, we obtained and processed a set of drill core samples from a drill hole that was logged from west to east near the surface outcrops at an

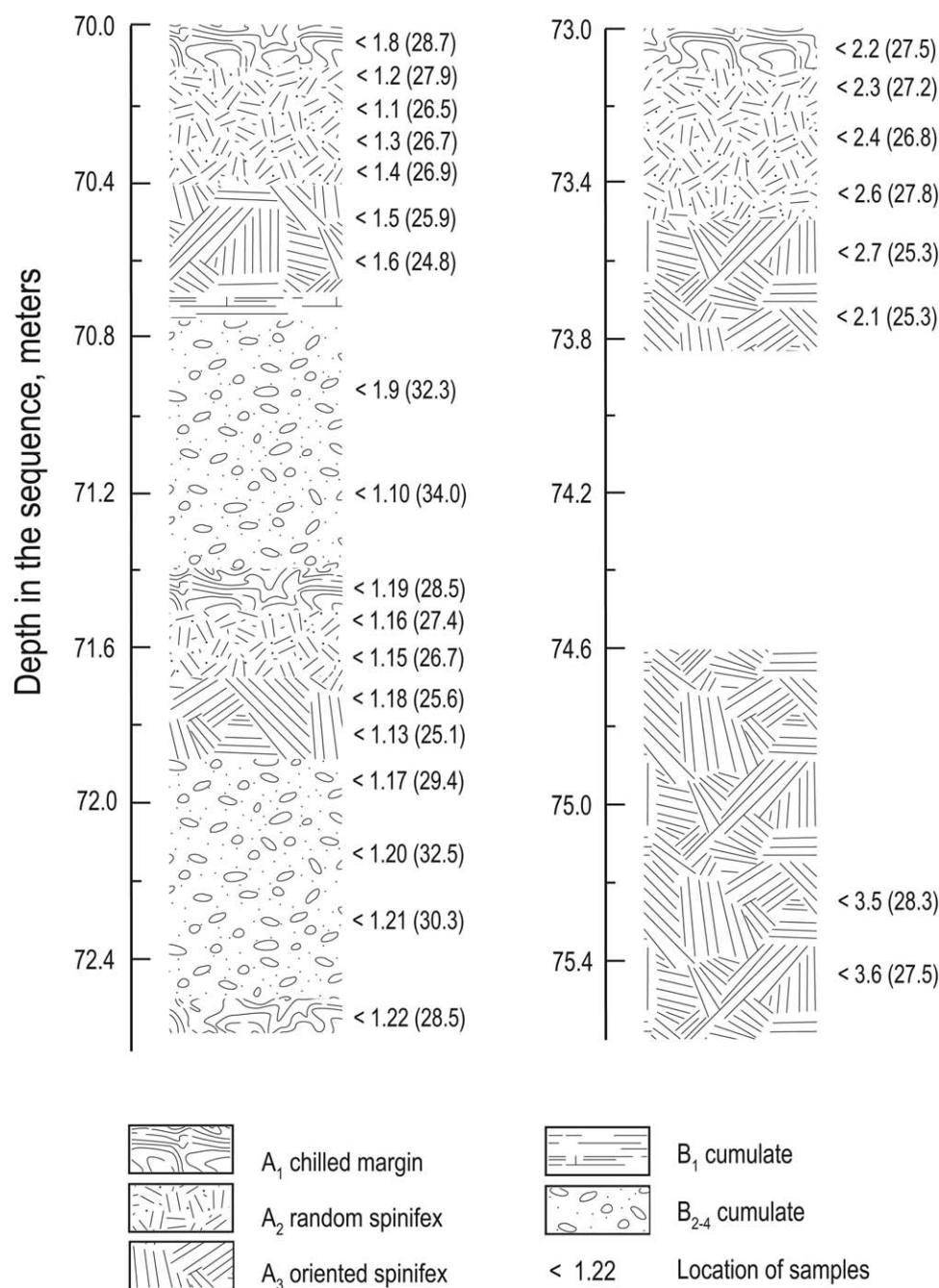


Figure 1. Schematic section of the Schapenburg komatiite lava sequence intersected by the drill hole logged near the surface outcrops of the Carl's and Patricia's lava flows and sampled in this study. Also shown are textural variations within the sampled lava flows, sample numbers, their location in the sequence, and MgO content (wt. %).

angle of approximately 45°E. It went through both the Carl's and Patricia's lava flows, and had a total length of 146 m. The interval sampled was between 70.0 and 75.5 m and included several differentiated komatiite lava flows (Figure 1). Texturally, these lava flows are similar to Carl's and Patricia's flows described in detail by Puchtel *et al.* [2009], and are characterized by a similar degree of preservation of the primary magmatic features. The purpose of the new sampling campaign was to: (1) obtain samples large enough to satisfy the requirements of the variety of isotopic and elemental abundance analyses carried out in this study, (2) replenish the material used in previous studies that had been exhausted, (3) obtain new, high-quality material suitable for W isotopic analysis using metal-free equipment, and (4) acquire high-precision ¹⁸⁷Re-¹⁸⁷Os,

$^{182}\text{W}/^{184}\text{W}$, $^{142,143}\text{Nd}/^{144}\text{Nd}$, and $^{176}\text{Lu}-^{176}\text{Hf}$ isotopic and W, lithophile trace element, and HSE abundance data, using state-of-the-art analytical techniques.

The age of the SGB komatiites has been constrained both indirectly, on the basis of analyses of magmatic zircons from felsic tuffs and lavas of the Theespruit Formation (3544 ± 2 to 3547 ± 3 Ma) [Kröner *et al.*, 1996], and directly, using the Re-Os chronometer (3549 ± 99 Ma) [Puchtel *et al.*, 2009].

Lécuyer *et al.* [1994] and Blichert-Toft *et al.* [2004] studied the lithophile trace element and isotopic characteristics of the SGR rocks. These authors concluded that, despite metamorphism and seafloor alteration, the komatiites have preserved most of their primary chemical and isotopic signatures. The $(\text{Gd}/\text{Yb})_{\text{N}} = 1.64 \pm 0.12$ and $\text{Al}_2\text{O}_3/\text{TiO}_2 = 11 \pm 2$ ratios were reported to be similar to the respective values for komatiites from the Komati Formation [Jahn *et al.*, 1982; Viljoen *et al.*, 1983; Lahaye *et al.*, 1995], which represents the type locality for the Barberton-type komatiites. Unlike the Komati komatiites, however, which have less-depleted light rare earth element (LREE) patterns and near-chondritic initial $\epsilon^{143}\text{Nd}$ [Jahn *et al.*, 1982; Puchtel *et al.*, 2013; Blichert-Toft *et al.*, 2015], the SGR komatiites are somewhat more depleted in LREE, with $(\text{La}/\text{Sm})_{\text{N}} = 0.91 \pm 0.06$, and are characterized by uniformly positive initial $\epsilon^{143}\text{Nd} = +2.5 \pm 0.2$ [Lécuyer *et al.*, 1994].

Previous study of the Lu-Hf isotope systematics in the SGR komatiites revealed high initial $\epsilon^{176}\text{Hf}$ values of up to +6, indicating that their mantle source evolved with time-integrated suprachondritic Lu/Hf [Blichert-Toft *et al.*, 2004]. This initial value stands in stark contrast to the near-chondritic initial $\epsilon^{176}\text{Hf}$ value obtained (in the same laboratory) by Puchtel *et al.* [2013] for the overlying Komati komatiites. The combination of the long-term elevated Lu/Hf in the Schapenburg komatiite source and the depletions of the Schapenburg komatiites in Al and heavy rare earth elements (HREEs) led Blichert-Toft *et al.* [2004] to propose a two-stage model for their formation. During the first very early stage, garnet accumulated in the source, creating a reservoir with suprachondritic Lu/Hf. This source remained isolated and evolved to high initial $\epsilon^{176}\text{Hf}$. During the second, partial melting stage, garnet was retained in the residue or fractionated from the resulting melt. The resultant magma was accordingly depleted in Al and HREE.

Puchtel *et al.* [2009] reported Re-Os isotope and HSE abundance data for the Schapenburg komatiites. These authors obtained a whole-rock Re-Os isochron age of 3549 ± 99 Ma and a radiogenic initial $\gamma^{187}\text{Os} = +3.7 \pm 0.3$, which they interpreted to reflect time-integrated suprachondritic $^{187}\text{Re}/^{188}\text{Os}$ in the source of the komatiites. The HSE abundances in the Schapenburg komatiites, except for Re and Pd, were found to be well correlated with indices of magmatic differentiation, such as MgO contents, and were calculated to be present in the mantle source of the komatiites in abundances of only ~25% of those in the BSE estimates of Becker *et al.* [2006]. In addition, the source of the Schapenburg komatiites was inferred to be characterized by a fractionated HSE pattern relative to BSE (including Re/Os). These unique characteristics of the Schapenburg komatiite source were interpreted to be the result of either fluid transport of radiogenic Os from a subducting slab, followed by incorporation into the overlying mantle and hydrous melting of the modified mantle to produce the komatiites, or dry melting of a chemically distinct, majorite-enriched mantle domain formed very early in Earth history as a result of initial stratification of the mantle during crystallization of a magma ocean [Puchtel *et al.*, 2009]. The authors concluded, however, that both models had their shortcomings in reconciling the available geochemical and petrological data for the Schapenburg komatiites.

3. Analytical Techniques

3.1. Sample Preparation

Each drill core sample, 400–600 g in weight, was split in quarters lengthwise using a diamond saw, and one quarter was used for further processing. Small slabs were cut from the quarters and thin sections were made at IGEM in Moscow. The remaining parts of the quarters were hand polished on all sides using SiC sandpaper to remove drill bit or saw marks, rinsed in Milli-Q water, dried, and crushed in an alumina-faced jaw crusher. A 100–150 g aliquot of crushed sample was ground in an alumina shatter box, finely reground in an alumina-faced disk mill, and used for the geochemical and isotopic studies.

3.2. Major and Trace Element Abundances

Major and minor element analyses were carried out at the Franklin and Marshall College on fused glass discs using a Phillips 2404 XRF vacuum spectrometer and following the protocol of *Mertzman* [2000]. Typical accuracy of the analyses was $\sim 2\%$ relative for major elements present in concentrations $>0.5\%$ and $\sim 5\%$ relative for the rest of the major and the minor elements as determined via analysis of USGS SRM BCR-1 and BIR-1 as unknowns [*Puchtel et al.*, 2016].

The abundances of the lithophile trace elements were determined using the standard addition solution inductively coupled plasma mass spectrometry technique (SA ICP-MS), as detailed in *Puchtel et al.* [2016]. Between 25 and 35 mg of sample powder, 0.5 mL double-distilled conc. HNO_3 , and 3 mL double-distilled conc. HF were sealed in 15 mL screw-cap Savillex Teflon vials and kept on a hotplate at 200°C for 48 h. The vials were opened, the sample solutions evaporated to dryness, and 0.5 mL of distilled conc. SeaStar HClO_4 added to the dry residue to convert fluorides into perchlorates. The vials were resealed and kept on a hotplate at 200°C for 24 h. The vials were reopened and the sample solutions dried down on a hotplate at 230°C . This step was followed by redissolution of the residue in 2 mL of 6 M HCl to convert it into the chloride form. This step was repeated until a clear solution with no visible precipitates was obtained. The dry residue was taken up in ~ 10 g of 0.8 M HNO_3 and this stock solution was used for preparing spiked aliquots for the ICP-MS measurements. A trace element standard addition spike was prepared containing concentrated mixed solutions of the trace elements to be analyzed. Three aliquots were taken for each sample with each aliquot containing ~ 1.0 g of the sample stock solution: to one aliquot no spike was added, to another spike amounting to 2X the estimated amount of element present in the sample aliquot was added, and to the last, spike amounting to 4X the estimated amount of element present in the sample aliquot was added. One total analytical blank (TAB) also was prepared and measured with each batch of six samples. Approximately 100 mg of 500 ppb In solution was added to each sample aliquot and the TAB solution to monitor and correct for signal drift during analysis, and the three solutions for each sample were diluted to 10 g with 0.8 M HNO_3 .

The sample solutions were analyzed on a *ThermoFisher Element 2* ICP-MS at the *Plasma Laboratory (PL)*, University of Maryland. Prior to analysis, the instrument was tuned to maximize sensitivity and minimize oxide production, and mass calibrated. The intensities of selected isotopes of each element were measured in low-resolution mode. The raw data were reduced using an in-house Excel macro. The in-run uncertainties on the concentrations were typically better than 1% for all elements (2SE). The external precision of the analyses was determined by analyzing multiple aliquots of the USGS SRM BIR-1 and BCR-1; for most elements, external precision was between 2 and 3% (2SD) and included the uncertainty introduced by sample powder heterogeneity.

3.3. Re-Os Isotopic Compositions and HSE Abundances

To obtain the Re-Os isotopic and HSE abundance data, ~ 1.5 g whole-rock powder, 6 mL purged, triple-distilled conc. HNO_3 , 4 mL triple-distilled conc. HCl, and appropriate amounts of mixed ^{185}Re - ^{190}Os and HSE (^{99}Ru , ^{105}Pd , ^{191}Ir , and ^{194}Pt) spikes were sealed in double internally cleaned, chilled 25 mL PyrexTM borosilicate Carius Tubes (CTs) and heated to 270°C for 96 h. Osmium was extracted from the acid solution by CCl_4 solvent extraction [*Cohen and Waters*, 1996], back extracted into HBr, and purified via microdistillation [*Birck et al.*, 1997]. Ruthenium, Pd, Re, Ir, and Pt were separated and purified using anion exchange chromatography. The TAB during the analytical session in which the studied batch of samples was processed was (in pg): Ru 2.8, Pd 6.4, Re 0.14, Os 0.35, Ir 0.16, and Pt 95 ($N = 1$). The TAB constituted less than 0.2% for Os, Ir, Ru, and Pd, 1.5–2.7% for Pt, and 0.4–4% for Re of the total element analyzed in the samples.

Osmium isotopic measurements were done via negative thermal ionization mass spectrometry (N-TIMS; *Creaser et al.* [1991]). All samples were analyzed using a secondary electron multiplier (SEM) detector of a *ThermoFisher Triton* mass spectrometer at the *Isotope Geochemistry Laboratory (IGL)*, University of Maryland. The measured isotopic ratios were corrected for mass fractionation using $^{192}\text{Os}/^{188}\text{Os} = 3.083$. The internal precision of measured $^{187}\text{Os}/^{188}\text{Os}$ for all samples was between 0.03% and 0.05% relative. The $^{187}\text{Os}/^{188}\text{Os}$ ratio of 300–500 pg loads of the in-house Johnson-Matthey Os standard measured during the 2 year period leading into the current analytical session averaged 0.11376 ± 10 (2SD, $N = 64$). This value characterizes the external precision of the isotopic analysis (0.1%), and was used to estimate the true uncertainty on the measured $^{187}\text{Os}/^{188}\text{Os}$ ratio for each individual sample. The measured $^{187}\text{Os}/^{188}\text{Os}$ ratios were further

corrected for instrumental mass bias relative to the average $^{187}\text{Os}/^{188}\text{Os} = 0.11379$ measured for the Johnson-Matthey Os standard on the Faraday cups of the *IGL Triton* [e.g., *Puchtel et al.*, 2014]. The correction factor of 1.00026 was calculated by dividing this value by the average $^{187}\text{Os}/^{188}\text{Os}$ measured for the Johnson-Matthey Os standard on the SEM of the same instrument.

The measurements of Ru, Pd, Re, Ir, and Pt were performed at the *PL* via ICP-MS using a *Nu Plasma* instrument with a triple electron multiplier configuration in static mode. Isotopic mass fractionation was monitored and corrected for by interspersing samples and standards. The accuracy of the data was assessed by comparing the results for the reference materials UB-N and GP-13 obtained during the ongoing analytical campaign [*Puchtel et al.*, 2014] with results from other laboratories. Concentrations of all HSE and Os isotopic compositions obtained at the *IGL* are in good agreement with data from other laboratories. Diluted spiked aliquots of iron meteorites were run during each analytical session as secondary standards. The results from these runs agreed within 0.5% for Re and Ir, and within 2% for Ru, Pt, and Pd, with fractionation-corrected values obtained from measurements of undiluted iron meteorites using Faraday cups on the same instrument with a signal of >100 mV for the minor isotopes. We therefore cite $\pm 2\%$ as the uncertainty on the concentrations of Ru, Pt, and Pd, $\pm 0.5\%$ as the uncertainty on the concentrations of Ir, and $\pm 0.2\%$ as the uncertainty on the concentrations of Os. Uncertainty on the Re concentrations was largely determined by the uncertainty on the variations in the TAB and was between 0.5 and 2%, assuming a $\sim 50\%$ variation in abundances of the TAB. The uncertainty on the Re concentration was the main source of uncertainty on the Re/Os ratio, and was estimated to be between 0.5 and 2%.

The regression calculations were performed using ISOPLOT 3.00 [*Ludwig*, 2003]. The uncertainties on the concentrations and isotopic ratios used for the regression calculations are those stated above. The initial $\gamma^{187}\text{Os}$ values were calculated as the per cent deviation of the isotopic composition at the time defined by the Re-Os isochron (3550 Ma) relative to the chondritic reference of *Shirey and Walker* [1998] at that time.

The average chondritic Os isotopic composition at the time defined by the isochron was calculated using the ^{187}Re decay constant $\lambda = 1.666 \times 10^{-11} \text{ year}^{-1}$, an early Solar System initial $^{187}\text{Os}/^{188}\text{Os} = 0.09531$ at $T = 4558 \text{ Ma}$, and $^{187}\text{Re}/^{188}\text{Os} = 0.40186$ [*Smoliar et al.*, 1996; *Shirey and Walker*, 1998].

3.4. Tungsten Isotopic Compositions and Abundances

The W isotope and concentration study was carried out at the *IGL* following the chemical procedures described in *Touboul et al.* [2014] for purifying W and measurement techniques developed by *Touboul and Walker* [2012] for determining W isotope compositions. For each isotopic analysis, about 1–2 g of sample was processed to obtain the $\sim 1 \mu\text{g}$ of W necessary for high-precision W isotope measurements. The sample powders were digested in 50 mL of a 5:1 mixture of double-distilled conc. HF and HNO_3 in 60 mL Savillex Teflon beakers on a hot plate at 150°C for 3–4 days and dried down. The residues were digested twice in a mixture of 20 mL conc. HNO_3 and 0.1 mL H_2O_2 at 120°C for 24 h and dried down. The residues were converted into the chloride form by repeated dissolutions in double-distilled 6 M HCl and subsequent dry downs. The residues were then redissolved in 10 mL of a mixture of 1 M HCl and 0.1 M HF. The sample solutions were centrifuged and the W in the supernatant was separated and purified using the four-stage ion exchange chromatography protocol described in *Touboul et al.* [2012], with minor modifications made to the procedure. The third stage involving a 1.5 mL anion exchange column was repeated to improve the separation of Ti from W, which significantly increased W ionization efficiency. Tungsten recovery using this procedure was better than 90% for all samples analyzed.

Tungsten isotopic compositions were measured by N-TIMS on the *ThermoFisher Triton* at the *IGL* using a two-line multistatic acquisition protocol and following the technique described by *Touboul and Walker* [2012]. This analytical technique permitted achievement of a ± 4.5 ppm external precision (2SD) on the $^{182}\text{W}/^{184}\text{W}$ ratio based on multiple measurements of the *Alfa Aesar* W standard solution carried out during each analytical session. Three separate digestions of the Hawaiian picrite sample H27 gave an average $\mu^{182}\text{W} = +1.0 \pm 1.6$ (2SD), where $\mu^{182}\text{W} = (((^{182}\text{W}/^{184}\text{W})_{\text{sample}} / (^{182}\text{W}/^{184}\text{W})_{\text{standard}} - 1) \times 10^6)$. Total procedural blanks averaged $\sim 1.8 \text{ ng}$, which was less than 0.2% of the total W present in the analyzed W cuts. Blank corrections on the measured W isotope compositions, therefore, were negligible.

Tungsten abundances were determined by isotope dilution ICP-MS. Between 100 and 200 mg of sample powder and a ^{182}W -enriched spike were equilibrated in 15 mL screw-cap Teflon vials using a 5:1 mixture of

double-distilled conc. HNO_3 and HF at 180°C for 3–4 days, followed by the dry down of the solutions. Residues were treated twice with double-distilled conc. HNO_3 and traces of H_2O_2 at 120°C for 24 h. After evaporation to dryness, residues were converted into the chloride form by adding 6 M HCl, followed by another dry down. Residues were then equilibrated with a 6 M HCl + 0.01 M HF mixture at 120°C for ~ 24 h, after which complete dissolution usually was achieved. Finally, solutions were dried down and residues redissolved in 2 mL of a 0.5 M HCl + 0.5 M HF mixture, and W purified using a previously established anion exchange chromatography technique [e.g., Kleine et al., 2004a].

The W isotopic compositions of the spiked samples were measured using the *Nu Plasma* ICP-MS at the PL. The total analytical blank for W averaged 170 ± 50 pg, corresponding to contributions of $<1\%$ of the total W present in the samples.

3.5. Sm-Nd Isotopic Compositions and Abundances

The Sm-Nd isotopic studies were carried out both at the IGL (the drill core samples) and at the *Department of Terrestrial Magnetism (DTM)*, Carnegie Institution for Science (the surface outcrop samples).

At IGL, the techniques outlined in Puchtel et al. [2013, 2016] were followed with some modifications. Between 200 and 300 mg of sample powder for each sample were sealed in a screw-cap 15 mL Teflon vessel with 5 mL double-distilled conc. HF and 1 mL double-distilled conc. HNO_3 and digested on a hotplate at 200°C for 24 h. The vessels were opened, the solutions dried down, and the digestion step repeated at 200°C for 48 h. After the solutions were again dried down, 0.5 mL of conc. SeaStar HClO_4 were added, the vials sealed and kept on a hotplate at 200°C for 24 h. The solutions were then dried down at $\sim 230^\circ\text{C}$, and the residues converted into the chloride form using 6 M HCl. This step was repeated twice. The residue was then taken up in 5 g of 2.5 M HCl and a 3% aliquot of the sample solution was weighed out and used for determination of the Sm and Nd concentrations via the standard addition ICP-MS technique described above. From the remaining 97% sample solution, REEs were first separated from the silicate matrix using standard cation exchange chromatography. The Nd fractions were further separated from the other REEs using first 2-methylactic acid cation exchange chromatography and then HDEHP extraction chromatography. The resultant Nd cuts were used for high-precision measurements of the Nd isotopic compositions.

Measurements of the Nd isotopic compositions were performed on the *ThermoFisher Triton* mass spectrometer at the IGL, using a two-line acquisition protocol and a multidynamic routine. For each sample load, between 2400 and 3600 ratios were collected with 8 s. integration times in blocks of 20 ratios each. For every three blocks of data collection, the two peaks were centered, the ion beam was refocused, and the amplifiers were electronically rotated relative to the Faraday cup detectors. A 30 s baseline measurement per block was performed for each Faraday cup/amplifier pair by beam deflection. The effects of instrumental mass fractionation were corrected relative to $^{146}\text{Nd}/^{144}\text{Nd} = 0.7219$ using an exponential law. A total of 10 loads of 900 ng of the Ames Nd standard were run at the beginning and end of the analytical session, with 2400 ratios collected during each measurement. During the measurements, the signal intensities for both the standards and the samples were kept at constant levels, between 3V and 5V on the ^{142}Nd mass. The calculated $^{147}\text{Sm}/^{144}\text{Nd}$ ratios were between 10^{-5} and 10^{-6} , meaning that corrections for Sm isobaric interferences were negligible. The calculated $^{142}\text{Ce}/^{142}\text{Nd}$ ratios were between 10^{-5} and 10^{-4} , resulting in interference corrections of >10 ppm on the $^{142}\text{Nd}/^{144}\text{Nd}$ ratio in some samples. No correlation between measured $^{142}\text{Nd}/^{144}\text{Nd}$ and the intensity of the ^{140}Ce signal was observed, indicating that these interferences were adequately corrected for. During the course of the present analytical campaign, the external reproducibility of the AMES Nd standard solution measurements was ± 2.8 ppm for $^{142}\text{Nd}/^{144}\text{Nd}$ and ± 3.5 ppm for $^{143}\text{Nd}/^{144}\text{Nd}$ (2SD, $N = 34$). The $^{142}\text{Nd}/^{144}\text{Nd}$ ratios are expressed in $\mu^{142}\text{Nd}$ units calculated as part per million (ppm) deviations from the average $^{142}\text{Nd}/^{144}\text{Nd}$ ratio of the AMES Nd standard obtained during the course of the analytical campaign.

The $^{147}\text{Sm}/^{144}\text{Nd}$ ratios used for calculating the initial $^{143}\text{Nd}/^{144}\text{Nd}$ isotopic ratios were determined using the standard addition ICP-MS technique described in detail in the section on major and lithophile trace elements. The precision and accuracy of determining the $^{147}\text{Sm}/^{144}\text{Nd}$ ratio was assessed by analyzing multiple aliquots of the USGS SRM BCR-1 and BIR-1. The average values obtained during the course of this analytical campaign were 0.1397 ± 8 ($N = 4$, 2SD) and 0.2798 ± 24 ($N = 18$, 2SD) for BCR-1 and BIR-1, respectively. The average $^{147}\text{Sm}/^{144}\text{Nd}$ ratio for BCR-1 is identical, within the uncertainty, to the average $^{147}\text{Sm}/^{144}\text{Nd} = 0.13939 \pm 16$ ($N = 4$, 2SD) obtained at the IGL using the ID-TIMS technique [Puchtel et al.,

2013]. The larger uncertainty on the $^{147}\text{Sm}/^{144}\text{Nd}$ ratio obtained for BIR-1 in this study (0.87% relative) compared to BCR-1 (0.55% relative) is ascribed to the inherently larger sample powder heterogeneity of BIR-1. As such, we use the external reproducibility of the $^{147}\text{Sm}/^{144}\text{Nd}$ ratio obtained for BCR-1 as a measure of uncertainty on the $^{147}\text{Sm}/^{144}\text{Nd}$ obtained in this study (0.5%, 2SD).

The initial $\epsilon^{143}\text{Nd}$ values were calculated based on the present-day parameters of the Chondritic Uniform Reservoir (CHUR): $^{147}\text{Sm}/^{144}\text{Nd} = 0.1967$ [Jacobsen and Wasserburg, 1980], $^{143}\text{Nd}/^{144}\text{Nd} = 0.512638$ [Hamilton et al., 1983].

At *DTM*, the analytical procedures were those given in Boyet and Carlson [2005] and Carlson et al. [2007]. Neodymium isotopic compositions were analyzed on a *ThermoFisher Triton* mass spectrometer using a 2-line dynamic acquisition routine. External reproducibility of $^{142}\text{Nd}/^{144}\text{Nd}$ measurements of the JNd-i standard was better than ± 4 ppm (2SD).

3.6. Lu-Hf Isotopic Compositions and Abundances

The Lu-Hf concentration and isotopic measurements were carried out at the Ecole Normale Supérieure in Lyon (*ENSL*), France. The sample dissolution procedure, employing Parr bombs and a mixed $>98\%$ pure ^{176}Lu - ^{180}Hf spike, and the Lu and Hf separation protocols used are described in Blichert-Toft et al. [1997], Blichert-Toft [2001], and Blichert-Toft and Puchtel [2010]. Lutetium and Hf isotopic compositions were measured by multicollector ICP-MS using the *Nu Plasma 500 HR* coupled with a *DSN-100* desolvating nebulizer and following the protocols of Blichert-Toft et al. [1997, 2002]. The JMC-475 Hf standard was analyzed every two samples and gave, during the present single analytical session, an average $^{176}\text{Hf}/^{177}\text{Hf} = 0.282164 \pm 0.000010$ (2SD; $N = 8$), which represents the best estimate of the external precision of the Hf isotope analyses (0.0035%). Since this value is identical, within errors, to the accepted value for the JMC-475 Hf standard of 0.282163 ± 0.000009 [Blichert-Toft and Albarède, 1997], no correction was applied to the data. We used the uncertainty obtained from the external reproducibility of the Hf standard as the uncertainty on the Hf isotopic composition for the isochron calculations, as all in-run precisions were either better than or equal to the external reproducibility. The uncertainty on the Lu/Hf ratio was 0.2% and this was the value we used for the isochron calculations for all samples. Total procedural blanks were <20 pg for both Lu and Hf.

For the isochron calculations, ISOPLOT 3.00 [Ludwig, 2003] and the ^{176}Lu decay constant of 1.867×10^{-11} year $^{-1}$ [Scherer et al., 2001; Söderlund et al., 2004] were used. The $\epsilon^{176}\text{Hf}$ values were calculated as parts per 10,000 deviation of the measured sample $^{176}\text{Hf}/^{177}\text{Hf}$ at the time of komatiite lava emplacement from the chondritic reference defined as $^{176}\text{Lu}/^{177}\text{Hf} = 0.0336$ and $^{176}\text{Hf}/^{177}\text{Hf} = 0.282785$ [Bouvier et al., 2008]. This set of reference parameters is identical within the quoted uncertainties to that of Blichert-Toft and Albarède [1997] for $^{176}\text{Hf}/^{177}\text{Hf}$ and nearly identical within the quoted uncertainties for $^{176}\text{Lu}/^{177}\text{Hf}$, hence allowing direct comparison of the present Lu-Hf isotope data set (on drill core samples) with that of Blichert-Toft et al. [2004] (on surface outcrop samples), who used the chondritic reference of Blichert-Toft and Albarède [1997].

4. Results

4.1. Major and Trace Element Abundances

The major and trace element abundances for the Schapenburg komatiite drill core samples are reported in Tables 1 and 2, and selected elements are plotted on variation diagrams in Figure 2, and as primitive mantle-normalized values in Figure 3. MgO contents vary between 27.5 and 28.7 wt.% in the A_1 zone samples (upper chilled margins), between 24.8 and 28.3 wt.% in the A_{2-3} zone samples (olivine spinifex), and between 29.4 and 36.0 wt.% in the B_{2-4} zone samples (olivine cumulates). Abundances of lithophile trace elements show well-defined inverse correlations with indices of magmatic differentiation, such as MgO contents; data for all petrogenetically important elements, except for W, plot with limited scatter on trends with negative slopes that coincide with olivine control lines, indicating magmatic olivine control of element abundance variations over the entire range of lava compositions (Figure 2). Tungsten abundances display significant scatter and do not define any significant correlation with MgO.

The primitive mantle-normalized patterns (Figure 3) are hump shaped with depletions in both light and heavy REE ($(\text{La}/\text{Sm})_N = 0.93 \pm 0.01$, $(\text{Gd}/\text{Yb})_N = 1.57 \pm 0.03$, 2SE) and large positive W anomalies. All samples are characterized by positive Nb anomalies ($\text{Nb}/\text{Nb}^* = 1.21 \pm 0.03$) and negative Zr and Hf anomalies relative to neighboring elements with similar compatibility during mantle melting. Based on the depletions in

Table 1. Major (wt.%) and Minor (ppm) Element Data for the Schapenburg Komatiites^a

Sample	SCH1.1	SCH1.2	SCH1.3	SCH1.4	SCH1.5	SCH1.6	SCH1.8	SCH1.9	SCH1.10	SCH1.13	SCH1.15	SCH1.16	SCH1.17
SiO ₂	47.7	47.2	46.8	46.2	47.1	47.8	47.4	46.3	45.3	47.7	47.5	47.4	45.6
TiO ₂	0.391	0.362	0.404	0.411	0.404	0.431	0.381	0.303	0.252	0.405	0.395	0.385	0.372
Al ₂ O ₃	4.10	3.69	3.92	4.14	4.18	4.13	3.59	3.16	2.71	3.93	3.70	3.71	3.80
Fe ₂ O ₃	11.9	13.2	13.3	13.5	13.1	12.6	11.6	11.9	11.3	12.3	12.7	12.6	13.8
MnO	0.180	0.161	0.202	0.191	0.182	0.170	0.221	0.171	0.182	0.192	0.172	0.203	0.201
MgO	26.5	27.9	26.7	26.9	25.9	24.8	28.7	32.3	36.0	25.1	26.7	27.4	29.4
CaO	8.14	6.60	7.59	7.58	8.16	8.97	7.15	5.02	3.64	9.26	7.85	7.31	5.81
Na ₂ O	0.44	0.32	0.45	0.44	0.47	0.50	0.37	0.19	0.14	0.47	0.43	0.43	0.39
K ₂ O	0.07	0.03	0.07	0.08	0.07	0.10	0.03	0.01	0.01	0.10	0.10	0.05	0.08
P ₂ O ₅	0.028	0.022	0.029	0.026	0.026	0.031	0.026	0.018	0.013	0.039	0.026	0.026	0.027
Cr	1982	1985	2071	2118	2079	2130	1907	1749	1557	2125	1995	1983	1863
Ni	1415	1651	1501	1492	1313	1280	1711	2268	2675	1219	1513	1518	1883
Total	99.83	99.47	99.11	99.70	99.08	99.75	99.77	99.14	99.23	98.78	98.83	98.66	99.51
LOI	4.15	5.12	3.52	3.39	2.80	2.48	4.13	7.09	8.27	3.10	3.82	3.17	5.21
Al ₂ O ₃ /TiO ₂	10.5	10.2	9.73	10.1	10.4	9.58	9.42	10.4	10.8	9.70	9.38	9.63	10.2
Sample	SCH1.18	SCH1.19	SCH1.20	SCH1.21	SCH1.22	SCH2.1	SCH2.2	SCH2.3	SCH2.4	SCH2.6	SCH2.7	SCH3.5	SCH3.6
SiO ₂	47.4	46.6	45.9	47.0	46.9	47.5	46.3	46.9	46.8	46.8	46.7	46.2	46.7
TiO ₂	0.446	0.392	0.289	0.362	0.402	0.428	0.389	0.389	0.409	0.369	0.421	0.389	0.380
Al ₂ O ₃	4.04	4.02	3.00	3.67	3.86	4.16	4.06	3.87	4.05	3.83	4.25	3.76	3.93
Fe ₂ O ₃	12.9	12.5	12.9	11.8	12.2	12.9	12.8	12.8	12.8	12.6	13.3	12.9	12.7
MnO	0.193	0.201	0.189	0.181	0.231	0.169	0.219	0.199	0.199	0.209	0.200	0.199	0.190
MgO	25.6	28.5	32.5	30.3	28.5	25.2	27.5	27.2	26.8	27.8	25.4	28.3	27.5
CaO	8.28	6.72	4.38	5.84	6.86	8.48	7.54	7.52	7.76	7.24	8.34	7.12	7.51
Na ₂ O	0.49	0.37	0.21	0.29	0.39	0.50	0.48	0.45	0.50	0.43	0.53	0.43	0.48
K ₂ O	0.09	0.13	0.01	0.02	0.06	0.07	0.07	0.09	0.11	0.08	0.27	0.04	0.05
P ₂ O ₅	0.033	0.029	0.017	0.029	0.021	0.031	0.034	0.032	0.035	0.034	0.047	0.04	0.03
Cr	2168	2012	1791	1864	1936	2074	1958	1950	2082	1898	2070	1977	1921
Ni	1361	1691	2278	2020	1678	1244	1561	1559	1499	1684	1347	1718	1690
Total	98.65	99.43	100.36	99.38	99.40	100.43	100.32	100.22	100.24	100.24	99.77	100.29	99.84
LOI	2.68	4.23	7.11	6.19	3.90	3.17	2.80	3.50	2.33	3.69	2.54	3.78	2.94
Al ₂ O ₃ /TiO ₂	9.07	10.3	10.4	10.1	9.60	9.72	10.4	9.95	9.90	10.4	10.1	9.67	10.3

^aNote: analyses were recalculated on an anhydrous basis, but not renormalized to 100% in order to preserve information on the quality of the analyses.

Table 2. Trace Element Data (ppm) for the Schapenburg Komatiites^a

Sample	SCH1.1	SCH1.5	SCH1.6	SCH1.9	SCH1.10	SCH1.20	SCH1.21	SCH2.1	SCH2.2	SCH2.3	SCH2.4	SCH2.6	SCH3.6
Th	0.104	0.107	0.120	0.0769	0.0746	0.0883	0.0869	0.121	0.105	0.116	0.100	0.0980	0.102
U	0.0359	0.0380	0.0392	0.0257	0.0222	0.0251	0.0255	0.0348	0.0314	0.0347	0.0337	0.0281	0.0298
Nb	1.44	1.41	1.54	1.12	0.839	1.11	1.22	1.49	1.41	1.41	1.39	1.33	1.32
La	1.64	1.79	1.99	1.23	0.962	1.18	1.42	1.72	1.65	1.65	1.62	1.63	1.60
Ce	4.59	4.94	5.62	3.42	2.70	3.32	3.91	5.21	4.86	4.69	4.67	4.52	4.55
Pr	0.693	0.763	0.847	0.528	0.420	0.513	0.609	0.763	0.722	0.710	0.722	0.698	0.697
Nd	3.56	3.85	4.24	2.71	2.12	2.63	3.12	3.85	3.65	3.71	3.60	3.48	3.47
Sm	1.11	1.18	1.29	0.846	0.647	0.806	0.965	1.18	1.13	1.13	1.11	1.07	1.06
Hf	0.646	0.634	0.684	0.472	0.413	0.433	0.572	0.696	0.625	0.616	0.643	0.587	0.622
Zr	23.9	23.6	23.9	17.1	14.2	16.0	19.3	23.9	21.9	22.6	21.9	21.1	20.9
Eu	0.370	0.457	0.501	0.275	0.222	0.279	0.319	0.445	0.436	0.451	0.454	0.419	0.429
Gd	1.40	1.47	1.64	1.07	0.828	1.03	1.22	1.50	1.42	1.45	1.40	1.34	1.32
Tb	0.225	0.237	0.261	0.171	0.132	0.163	0.197	0.241	0.232	0.230	0.230	0.216	0.212
Dy	1.43	1.48	1.67	1.08	0.841	1.03	1.26	1.53	1.46	1.47	1.43	1.37	1.35
Y	7.12	7.48	7.95	5.33	4.32	5.41	6.00	7.56	6.93	7.10	7.35	6.78	6.94
Ho	0.287	0.301	0.326	0.219	0.170	0.212	0.254	0.309	0.291	0.299	0.291	0.275	0.275
Er	0.747	0.766	0.849	0.564	0.447	0.559	0.644	0.801	0.754	0.759	0.762	0.723	0.706
Tm	0.113	0.115	0.130	0.0844	0.0674	0.0855	0.0952	0.122	0.114	0.116	0.114	0.111	0.107
Yb	0.715	0.721	0.841	0.539	0.443	0.565	0.602	0.787	0.726	0.742	0.734	0.709	0.686
Lu	0.103	0.102	0.120	0.0788	0.0654	0.0836	0.0863	0.114	0.104	0.105	0.104	0.101	0.0982
Ti/Zr	97.8	103	108	106	107	108	112	107	106	103	112	105	109
Nb/Nb*	1.26	1.16	1.14	1.32	1.13	1.24	1.26	1.18	1.23	1.16	1.25	1.20	1.18
(La/Sm) _N	0.934	0.956	0.968	0.915	0.936	0.919	0.928	0.913	0.918	0.919	0.922	0.961	0.954
(Gd/Yb) _N	1.58	1.65	1.57	1.61	1.51	1.48	1.64	1.54	1.58	1.57	1.54	1.53	1.56

^aNote: analyses were recalculated on an anhydrous basis. N—normalized to the BSE values of Hofmann [1988].

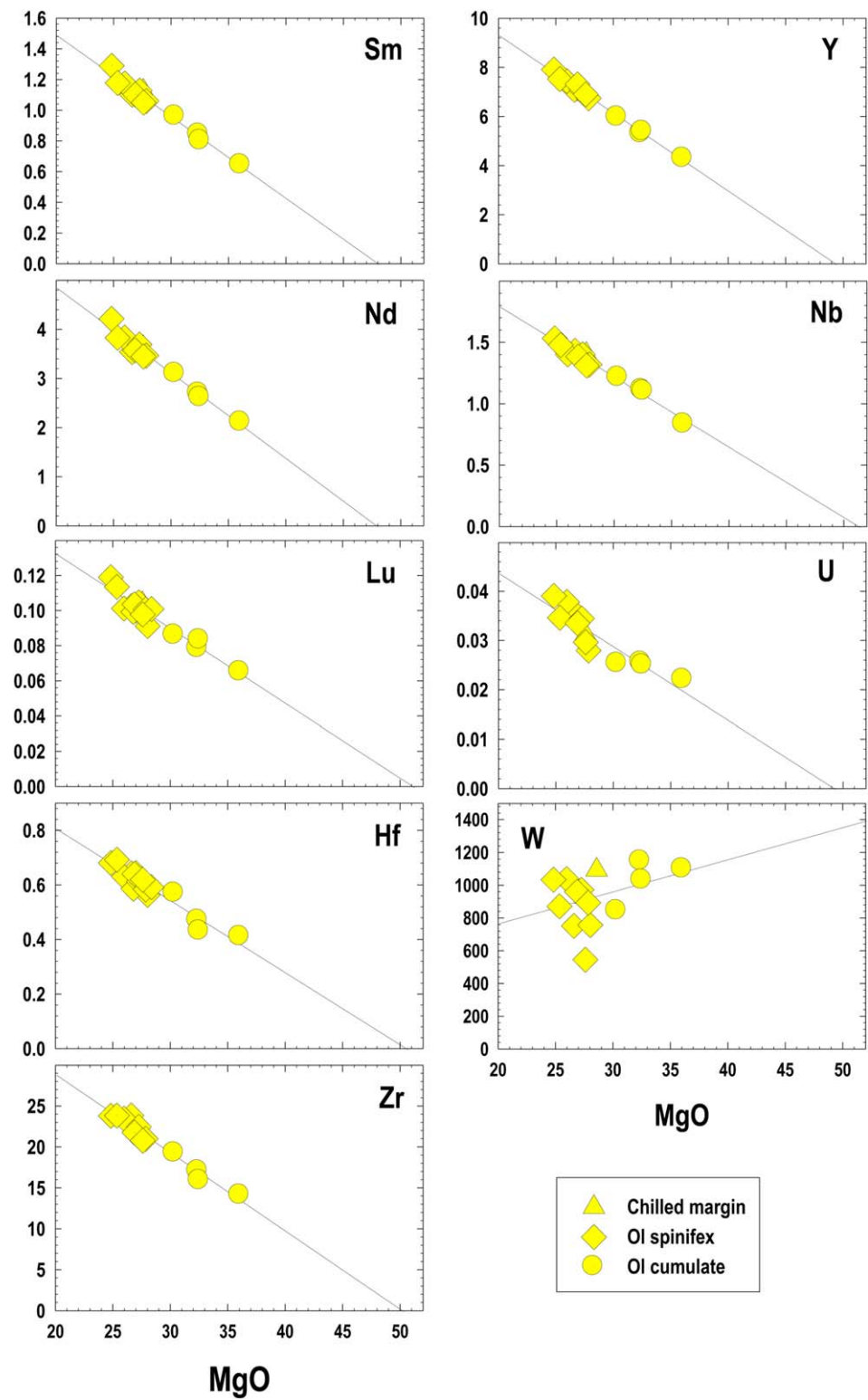


Figure 2. Abundances of selected lithophile trace elements (ppm) and W (ppb) obtained in this study plotted against MgO (wt.%) contents in the Schapenburg komatiites.

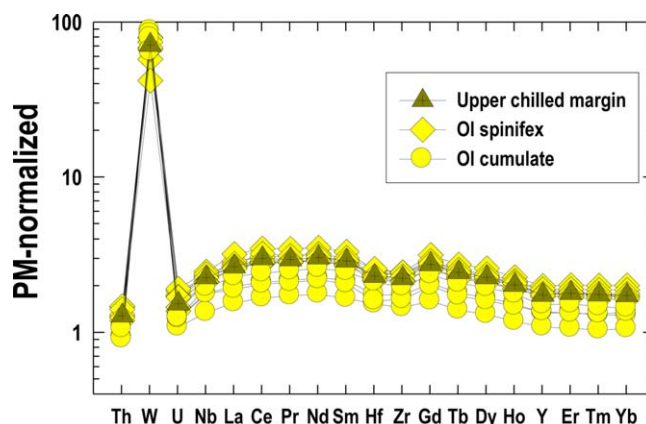


Figure 3. BSE-normalized abundances of lithophile trace elements in the Schapenburg komatiites obtained in this study arranged in decreasing order of incompatibility during mantle melting. The normalizing values for W are from Arevalo and McDonough [2008] and for the rest of the elements from Hofmann [1988].

HREE and Al ($Al_2O_3/TiO_2 = 10.0 \pm 0.2$), the Schapenburg komatiites belong to the Al-depleted-type lavas of Nesbitt *et al.* [1979] and Jahn *et al.* [1982]; they also are ~15% more depleted in HREE than the type locality komatiites from the Komati Formation of the BGB ($(Gd/Yb)_N = 1.38 \pm 0.02$, Puchtel *et al.* [2013]).

4.2. Re-Os Isotopic Compositions and HSE Abundances

The new Re-Os isotopic and HSE abundance data for the Schapenburg komatiites are presented in Table 3 and, together with the data for the surface outcrop samples from Puchtel *et al.* [2009], plotted on the Re-Os isochron diagram in Figure 4 and on the

MgO versus HSE variation diagrams in Figure 5. A total of 18 spinifex-textured and olivine cumulate samples define an isochron with a slope corresponding to an ISOPLLOT Model 3 [Ludwig, 2003] age of 3550 ± 87 Ma and an initial $^{187}Os/^{188}Os = 0.10630 \pm 26$ ($\gamma^{187}Os = +3.7 \pm 0.2$). Both the age and the initial Os isotopic ratio obtained in this study are identical to those reported for the surface outcrop samples studied by Puchtel *et al.* [2009], although regression of the combined data yields more precise results.

The HSE abundances in the drill core samples are generally similar to those in the surface outcrop samples from Puchtel *et al.* [2009], but plot on tighter trends in the MgO versus HSE variation diagrams (Figure 5). The largest difference is observed for Pd; the data for the drill core samples define a strong correlation with MgO contents, whereas the surface outcrop samples plot with significant scatter, likely due to the stronger effects of oxidative weathering on Pd, as was also argued by Puchtel *et al.* [2007] for the 2.9 Ga Sumozero-Kenozero komatiites. Osmium, Ir, and Ru concentrations show a broad pattern of decreasing abundances with increasing MgO contents, typical of the so-called Kostomuksha-type lavas characterized by undersaturation of their parental komatiite magmas in Os-Ir alloys [Puchtel and Humayun, 2005]. Osmium abundances in the drill core samples plot on a trend that is slightly offset to lower abundances compared to the trend defined by the surface outcrop samples. Since all samples with two exceptions plot on the Re-Os isochron, it is unlikely that this displacement resulted from the effects of secondary alteration; more likely, it is due to small inherent variations in the Os abundances in different lava flows within the Schapenburg komatiite lava sequence. Platinum and Pd abundances show strong negative correlations with MgO contents and plot on trends that coincide with olivine control lines, indicating olivine control over the entire range of the komatiite compositions and also attesting to the immobile behavior of these elements during secondary processes. By contrast, Re abundances, in both drill core and surface outcrop samples, plot with significant scatter, indicating mobility of Re during seafloor alteration and/or metamorphism of the Schapenburg komatiites.

Applying the protocol originally devised for the Puchtel *et al.* [2004] study of the Abitibi komatiites, and refined in later studies [e.g., Puchtel *et al.*, 2014], to the new, tighter correlations defined by the HSE

Table 3. HSE Abundances (ppb), Re-Os Isotopic Data, and Elemental Ratios for the Schapenburg Komatiites^a

Sample	Re	Os	Ir	Ru	Pt	Pd	$^{187}Re/^{188}Os$	$^{187}Os/^{188}Os$	$\gamma^{187}Os(T)$	$(Os/Ir)_N$	$(Ru/Ir)_N$	$(Pd/Ir)_N$
SCH2.6	0.0231	0.9825	0.810	2.367	3.546	3.954	0.1133 ± 6	0.11276 ± 5	+3.2	1.18	2.00	3.81
SCH1.5	0.0315	1.003	0.832	2.318	3.864	4.086	0.1512 ± 8	0.11526 ± 6	+3.4	1.17	1.90	3.84
SCH1.6	0.0148	1.080	0.900	2.314	3.939	4.373	0.0657 ± 8	0.11010 ± 5	+3.5	1.16	1.76	3.79
SCH1.9	0.00912	0.8305	0.768	2.276	2.811	2.977	0.0528 ± 10	0.10969 ± 6	+3.8	1.05	2.03	3.03
SCH1.10	0.0121	0.7541	0.696	2.194	2.490	2.568	0.0773 ± 11	0.11121 ± 5	+3.9	1.05	2.15	2.88

^aNote: the HSE abundances are recalculated on an anhydrous basis. The initial $\gamma^{187}Os$ values were calculated for $T = 3550$ Ma defined by the Re-Os isochron and using the parameters specified in the text. The normalizing values are from Horan *et al.* [2003].

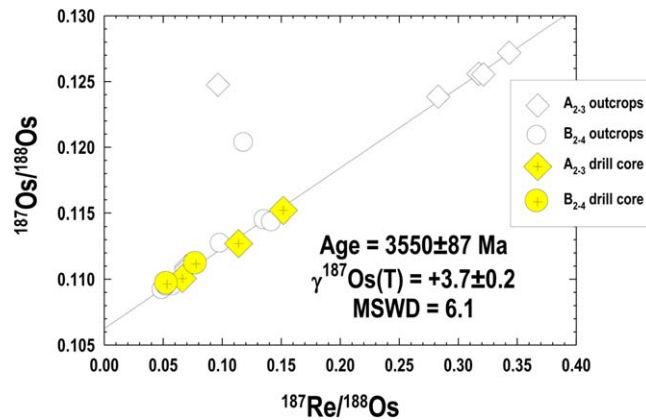


Figure 4. Combined Re-Os isochron diagram for the Schapenburg komatiites. Results of the regression analysis are based on the data from both *Puchtel et al.* [2009] (surface outcrop samples) and this study (drill core samples).

abundance data in the drill core samples (Figure 5), the Pt and Pd abundances in the source of the Schapenburg komatiites were estimated. As discussed by these authors, one of the prerequisites for this protocol to be applicable to calculating the Pt and Pd abundances in the mantle source of a komatiite lava from the measured komatiite Pt and Pd abundances is the complete exhaustion of sulfides harboring Pt and Pd in the source, which can safely be assumed at the degrees of partial melting typical of komatiites (>20-25%: *Barnes et al.* [1985] and *Keays* [1995]). As will be discussed later, the Schapenburg komatiites are estimated to have formed via >20%

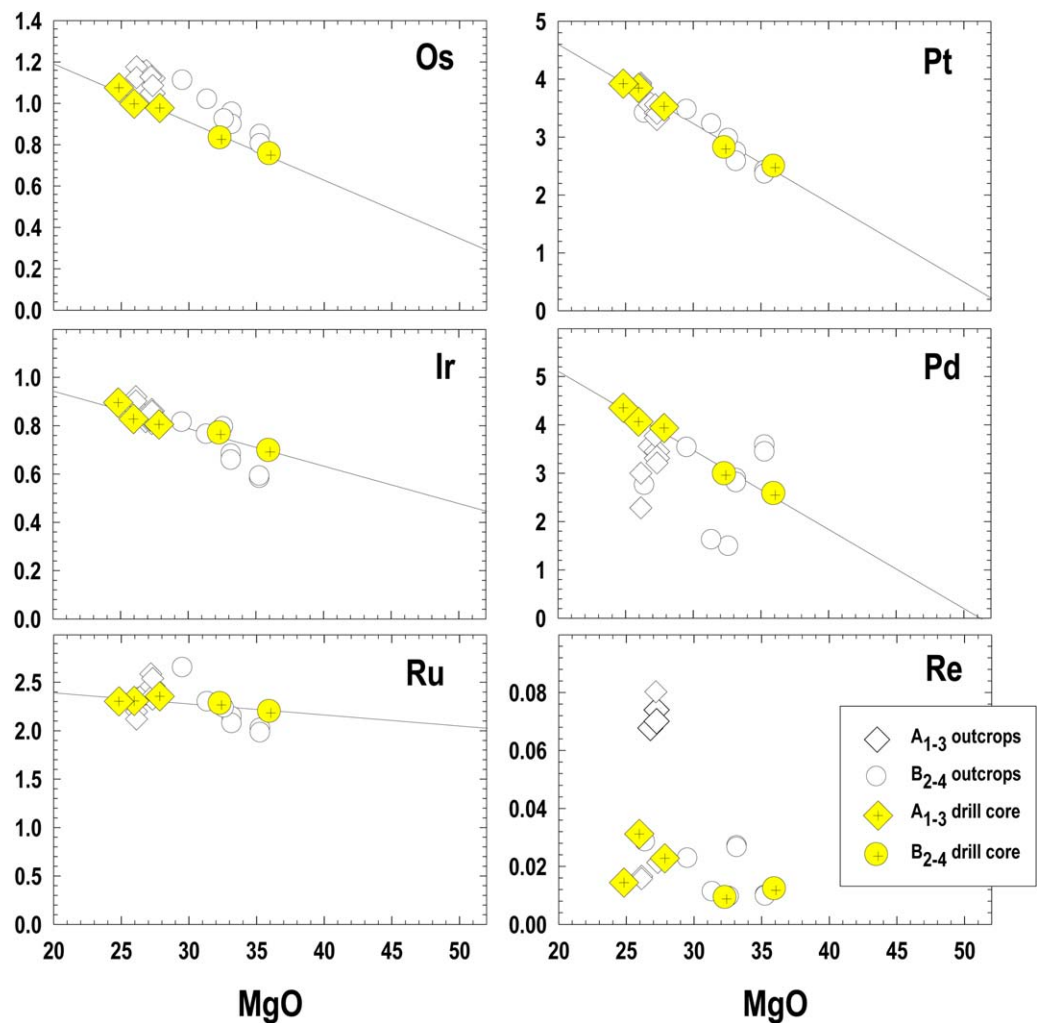


Figure 5. Abundances of the highly siderophile elements in the Schapenburg komatiites (ppb) obtained in the *Puchtel et al.* [2009] study (surface outcrop samples) and this study (drill core samples) plotted against MgO contents (wt.%). The regressions are done on the data obtained on the drill core samples from this study only.

Table 4. Tungsten Abundances and Isotopic Compositions for the Schapenburg Komatiites and Hawaiian Picrite H27^a

Sample	W (ppb)	$\mu^{182}\text{W}$
SCH1.1	727 ± 7	
SCH1.2	726 ± 7	
SCH1.5	1015 ± 10	-6.4 ± 3.2
SCH1.6	1014 ± 10	
SCH1.9	1074 ± 11	-10.4 ± 1.5
Replicate		-12.4 ± 2.5
SCH1.10	1019 ± 10	-8.2 ± 2.4
SCH1.19	1055 ± 11	-8.7 ± 1.9
SCH1.20	966 ± 10	
SCH1.21	798 ± 8	-6.9 ± 2.5
SCH 2.1	849 ± 8	-6.3 ± 3.1
SCH 2.2	908 ± 9	-10.2 ± 2.0
SCH 2.3	944 ± 9	
SCH 2.4	943 ± 9	
SCH 2.6	866 ± 9	-6.5 ± 1.7
SCH 3.6	535 ± 5	-7.8 ± 2.1
H27_M0269		+0.3 ± 3.8
H27_M0284		+1.8 ± 5.2
H27_M0342		+1.0 ± 4.5

^aNote: uncertainties on W abundances are 2SE. Uncertainties on isotopic compositions for individual samples are the 2SE run statistics of the individual analyses. The data for the Hawaiian picrite H27 were obtained on three separate digestions over the course of the entire analytical campaign.

partial melting of an already depleted mantle source, and, therefore, were most likely sulfide-undersaturated prior to emplacement, with even stronger evidence for the sulfide-undersaturated nature of the Schapenburg primary komatiite lava provided by the incompatible behavior of Pd during lava differentiation (Figure 5).

The next step in calculating the Pt and Pd abundances in the source of the Schapenburg parental komatiite magma is to conduct an ISOPLOT regression analysis using the Pt, Pd, and MgO abundance data for individual samples and respective analytical uncertainties on these concentrations and then calculate the Pt and Pd abundances for the assumed MgO content of the mantle source of 38 wt.%. These calculations yield Pt and Pd abundances in the Schapenburg komatiite source of 2.12 ± 0.36 and 2.15 ± 0.40 ppb, respectively. The total Pt and Pd abundances in the source of the Schapenburg komatiites are, thus, calculated to be only 29 ± 5% of those in the estimates for the modern BSE of Becker *et al.* [2006]. The uncertainty on this value is largely defined by the uncertainty of the regression calculations.

4.3. W Isotopic Compositions and Abundances

Tungsten abundances and isotopic compositions of the Schapenburg komatiites are listed in Table 4 and plotted in Figures 2, 3, and 6. The W abundances vary from 535 to 1040 ppb. Such high W abundances are unlikely to have resulted from direct partial melting of rocks with W abundances in the range of 12–13 ppb estimated for the BSE [Arevalo and McDonough, 2008; König *et al.*, 2011]. Furthermore, although W is a highly incompatible trace element, and should behave in a manner similar to other incompatible lithophile trace elements, W concentrations do not correlate with chemical indicators of magmatic differentiation typical of komatiitic systems, such as MgO content (Figure 2), and also exhibit large positive anomalies on the BSE-normalized plots relative to elements with similar incompatibility during mantle melting and differentiation processes (Figure 3).

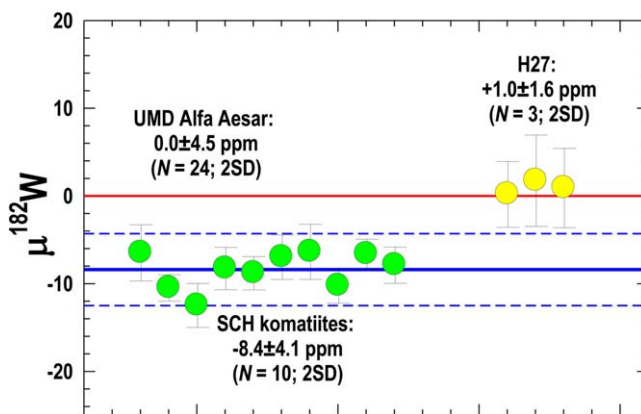


Figure 6. Tungsten isotopic compositions of komatiites from the 3.55 Ga Schapenburg Greenstone Remnant. The data are reported in $\mu^{182}\text{W}$ units, which are parts per million (ppm) deviations of the $^{182}\text{W}/^{184}\text{W}$ ratio of a given sample relative to the mean $^{182}\text{W}/^{184}\text{W}$ ratio measured for the Alfa Aesar W standard. Each symbol corresponds to an individual sample. Data for three separate measurements of the Hawaiian picrite sample H27 are provided for reference.

Despite the considerable, seemingly irregular, variations in W concentrations, all the komatiite samples analyzed are characterized by uniformly depleted $^{182}\text{W}/^{184}\text{W}$ ratios. Collectively, the isotopic data define an average $\mu^{182}\text{W}$ value of -8.4 ± 1.6 (2SE, $n = 10$), where $\mu^{182}\text{W}$ is the parts per million deviation of $^{182}\text{W}/^{184}\text{W}$ of a given sample from that of terrestrial standards and modern mantle rocks, the latter two of which are identical and, by definition, equal to zero (Table 4 and Figure 6). This negative ^{182}W

Table 5. Sm-Nd Isotope and Concentration Data for the Schapenburg Komatiites and the USGS SRM BCR-1^a

Sample	Sm (ppm)	Nd (ppm)	¹⁴⁷ Sm/ ¹⁴⁴ Nd	±2SE	¹⁴³ Nd/ ¹⁴⁴ Nd	±2SE	ε ¹⁴³ Nd(T)	μ ¹⁴² Nd
SCH1.1	1.063**	3.418**	0.1880	0.0004	0.512522	0.000001	+1.7	-2.8 ± 2.2
Replicate*					0.512525	0.000002		-6.0 ± 2.1
SCH1.5	1.148	3.749	0.1851	0.0004	0.512473	0.000003	+2.1	
Replicate					0.512475	0.000001		-5.5 ± 1.8
SCH1.6	1.263	4.133	0.1848	0.0004	0.512469	0.000002	+2.2	-8.0 ± 2.4
SCH2.1	1.081	3.545	0.1844	0.0004	0.512474	0.000001	+2.5	-4.5 ± 1.9
Replicate					0.512475	0.000001		-7.1 ± 2.6
SCH2.2	1.100	3.551	0.1873	0.0004	0.512519	0.000003	+2.0	-6.6 ± 4.6
Replicate					0.512520	0.000001		-4.4 ± 1.9
SCH2.3	1.050	3.429	0.1851	0.0004	0.512501	0.000002	+2.7	-7.2 ± 5.1
Replicate	1.004	3.271	0.1856	0.0004	0.512496	0.000003	+2.3	
Replicate					0.512499	0.000002		-2.5 ± 2.3
SCH2.4	1.083	3.513	0.1863	0.0004	0.512521	0.000001	+2.5	-2.1 ± 2.0
SCH2.6	1.027	3.360	0.1849	0.0004	0.512495	0.000001	+2.6	-7.9 ± 1.8
SCH3.6	1.025	3.369	0.1840	0.0004	0.512468	0.000001	+2.5	-1.6 ± 1.5
P-3					0.512509	0.000002		-13.4 ± 3.9
P-4					0.512500	0.000004		-3.0 ± 7.7
P-4					0.512498	0.000003		-2.0 ± 4.8
P-5					0.512512	0.000002		-4.2 ± 3.8
C-4					0.512504	0.000003		-3.8 ± 4.5
C-5					0.512477	0.000003		-3.9 ± 4.7
C-6					0.512519	0.000002		-4.0 ± 3.6
BCR-1_1					0.512645	0.000002		+1.1 ± 2.5
BCR-1_2					0.512645	0.000001		+0.3 ± 1.7
BCR-1_3					0.512644	0.000002		+0.7 ± 3.6

^aNote: *replicate digestions of the samples. **Sm and Nd abundances were determined on ~3% aliquots of the same sample digestions done for the high-precision Nd isotopic analyses, using the SA ICP-MS technique, as specified in the text. Drill core SCH samples were run at the JGL, while surface outcrop samples P3 through C6 were run at DTM. Initial ε¹⁴³Nd values were calculated for the age *T* = 3550 Ma defined by the Re-Os isochron based on the combined data from Puchtel *et al.* [2009] and this study. The data for the USGS SRM BCR-1 were obtained on three separate digestions over the course of the entire analytical campaign.

anomaly is the first reported to date for terrestrial rocks and contrasts with the positive anomaly reported for the 2.8 Ga Kostomuksha komatiites [Touboul *et al.*, 2012].

4.4. Sm-Nd and Lu-Hf Isotopic Compositions and Abundances

The Sm-Nd isotopic data are provided in Table 5. All Schapenburg komatiites analyzed are characterized by ¹⁴²Nd deficits, with an average μ¹⁴²Nd = -5.0 ± 1.3 (2SE, *n* = 20), where μ¹⁴²Nd is the parts per million deviation of ¹⁴²Nd/¹⁴⁴Nd of a given sample from that of terrestrial standards and modern mantle rocks, the latter two of which are identical and, by definition, equal to zero (Table 5 and Figure 7). The only other terrestrial rocks reported so far to have ¹⁴²Nd deficits are from Earth's oldest known crustal segments, Nuvvuagittuq in Québec, Isua in West Greenland, and Acasta in the Northwest Territories [O'Neil *et al.*, 2008; Rizo *et al.*, 2012, 2013; Roth *et al.*, 2013, 2014].

The long-lived lithophile isotope systems provide some seemingly conflicting information. The new ¹⁴⁷Sm-¹⁴³Nd data for the Schapenburg komatiites of this study, combined with the data reported by Lécuyer *et al.* [1994], yield an isochron age of 3480 ± 530 Ma (MSWD = 1.3), consistent with the Re-Os isochron age on the same samples reported above. This indicates that the rocks behaved essentially as closed systems with regard to their Sm-Nd isotope systematics, as also evidenced by the magmatic nature of the Sm and Nd abundance variations as a function of MgO content (Figure 2). The limited variation in Sm/Nd among the present samples precludes generation of a precise isochron, although a precise initial ε¹⁴³Nd = +2.4 ± 0.1 (2SE, *n* = 21), where ε¹⁴³Nd is the parts per 10,000 deviation of the ¹⁴³Nd/¹⁴⁴Nd ratio of a given sample from the chondritic, or BSE, reference value, is obtained by averaging the initial ¹⁴³Nd/¹⁴⁴Nd ratios calculated using the measured sample ¹⁴⁷Sm/¹⁴⁴Nd and ¹⁴³Nd/¹⁴⁴Nd ratios and the komatiite emplacement age of 3550 Ma. There is, thus, an apparent decoupling between the short-lived ¹⁴⁶Sm-¹⁴²Nd system, with a negative deviation, and the ¹⁴⁷Sm-¹⁴³Nd system with a positive deviation from the BSE benchmark. The calculated initial ¹⁴³Nd enrichment in the Schapenburg komatiite system is generally comparable to projections of the Depleted MORB Mantle (DMM) to that time (present-day ¹⁴³Nd/¹⁴⁴Nd = 0.513151, ¹⁴⁷Sm/¹⁴⁴Nd = 0.2135, ε¹⁴³Nd_{DMM}(0) = +10) [Bennett, 2003].

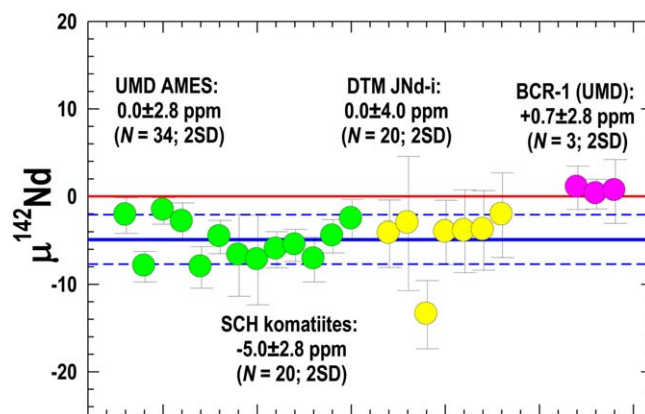


Figure 7. Neodymium isotopic compositions of komatiites from the 3.55 Ga Schapenburg Greenstone Remnant. The data are reported in $\epsilon^{142}\text{Nd}$ units, which are parts per million (ppm) deviations of the $^{142}\text{Nd}/^{144}\text{Nd}$ ratio of a given sample relative to the mean $^{142}\text{Nd}/^{144}\text{Nd}$ ratio measured for the AMES Nd standard. Each symbol corresponds to an individual sample. Green symbols represent data for the drill core samples measured at the IGL, while yellow symbols represent data for the surface outcrop whole-rock samples from Patricia’s and Carl’s flows analyzed at DTM. Data for three separate measurements of the USGS SRM BCR-1 are provided for reference.

The new ^{176}Lu - ^{176}Hf data obtained for the Schapenburg komatiites in this study, combined with the data from *Blichert-Toft et al.* [2004], define a broad correlation in $^{176}\text{Hf}/^{177}\text{Hf}$ - $^{176}\text{Lu}/^{177}\text{Hf}$ space corresponding to an age of 3167 ± 290 Ma (MSWD = 1.7), which also overlaps, within the uncertainties, the Re-Os isochron age. As with the Sm-Nd system, the limited range in Lu/Hf precludes determination of a more precise age. The initial $\epsilon^{176}\text{Hf}$ of individual samples from this study and that of *Blichert-Toft et al.* [2004], calculated assuming a 3.55 Ga komatiite emplacement age, define a precise average initial $\epsilon^{176}\text{Hf} = +5.7 \pm 0.3$ (2SE, $n = 17$), where $\epsilon^{176}\text{Hf}$ is the parts per 10,000 deviation of the $^{176}\text{Hf}/^{177}\text{Hf}$ ratio of a given sample from the chondritic reference value (Table 6). The calculated

initial ^{176}Hf enrichment is 1.5 $\epsilon^{176}\text{Hf}$ units higher than projections of the DMM to that time ($\epsilon^{176}\text{Hf}_{\text{DMM}}(3550) = +4.2$, present-day $^{176}\text{Hf}/^{177}\text{Hf} = 0.283294$, $^{176}\text{Lu}/^{177}\text{Hf} = 0.0393$, $\epsilon^{176}\text{Hf}_{\text{DMM}}(0) = +18$) [*Bouvier et al.*, 2008; *Blichert-Toft and Puchtel*, 2010], and, thus, plots well above the Nd-Hf terrestrial array (Figure 8).

5. Discussion

5.1. The Source of W in the Schapenburg Komatiites

Two initial issues that must be addressed regarding the Schapenburg komatiites are the relatively high W concentrations and the lack of correlation between W abundances and indicators of magmatic evolution, such as MgO. Unlike, for example, U abundances, W abundances do not correlate with MgO despite broadly similar degrees of incompatibility of U and W during mantle melting and susceptibility to mobility during fluid-rock interaction. Although W abundance data for each individual lava flow are limited, there is little to no evidence for negative within-flow correlations with MgO contents. This conspicuous lack of correlation suggests that the behavior of W in the studied differentiated lava flows was controlled not by olivine, but by other, yet unidentified, phase(s). Tungsten concentrations in the Schapenburg komatiites systematically exceed 500 ppb, substantially higher than would be expected for ultramafic lavas produced by high

Table 6. Lu-Hf Isotope and Concentration Data for the Schapenburg Komatiites^a

Sample	Lu (ppm)	Hf (ppm)	$^{176}\text{Lu}/^{177}\text{Hf}$	$\pm 2\text{SE}$	$^{176}\text{Hf}/^{177}\text{Hf}$	$\pm 2\text{SE}$	$\epsilon^{176}\text{Hf}(\text{T})$
SCH1.2	0.08722	0.5392	0.02296	0.00011	0.282219	0.000003	+5.8
SCH1.4	0.09728	0.6252	0.02208	0.00011	0.282171	0.000003	+6.2
SCH1.9	0.07201	0.4410	0.02317	0.00012	0.282227	0.000009	+5.6
SCH1.15	0.09608	0.5677	0.02402	0.00012	0.282291	0.000012	+5.8
SCH1.17	0.07393	0.4989	0.02103	0.00011	0.282106	0.000003	+6.5
SCH1.21	0.08120	0.5385	0.02140	0.00011	0.282123	0.000003	+6.2
SCH2.2	0.1005	0.6079	0.02345	0.00012	0.282243	0.000007	+5.4
SCH2.3	0.09806	0.5951	0.02339	0.00012	0.282258	0.000008	+6.1
SCH2.4	0.1081	0.6285	0.02440	0.00012	0.282285	0.000004	+4.6
SCH2.6	0.09694	0.5657	0.02432	0.00012	0.282297	0.000005	+5.3
SCH3.5	0.09767	0.5734	0.02418	0.00012	0.282277	0.000004	+4.9
SCH3.6	0.09887	0.6045	0.02321	0.00012	0.282246	0.000004	+5.4

^aNote: initial $\epsilon^{176}\text{Hf}$ values were calculated for the age $T = 3550$ Ma defined by the combined Re-Os isochron based on the data from *Puchtel et al.* [2009] and this study, using the parameters specified in the text.

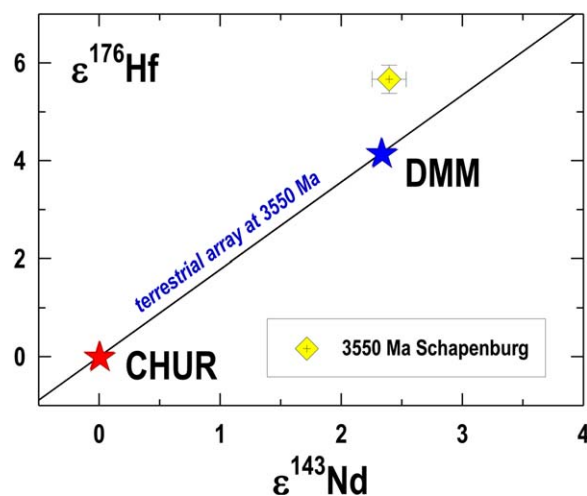


Figure 8. Diagram illustrating the $\epsilon^{143}\text{Nd}$ and $\epsilon^{176}\text{Hf}$ values for the mantle source of the Schapenburg komatiites and the Chondritic Uniform Reservoir (CHUR) and Depleted MORB Mantle (DMM) calculated at the time of komatiite emplacement (3550 Ma). The CHUR and DMM parameters are from Jacobsen and Wasserburg [1980], Hamilton et al. [1983], Goldstein et al. [1984], Vervoort and Blichert-Toft [1999], Bouvier et al. [2008], and Blichert-Toft and Puchtel [2010]. Note the decoupling of, or incongruence between, the two isotope systems in the source of the Schapenburg komatiites resulting in the data plotting well above the terrestrial array.

the selective remobilization and transport of W into mantle wedge settings by subduction zone fluids [König et al., 2008]. However, W/Th and W/U ratios in the Schapenburg komatiites are considerably higher than reported for any arc-related magmatic rocks. Further, no other chemical evidence ties the Schapenburg komatiites to a subduction zone environment, unlike some other locations. For example, aqueous transfer of ^{182}W -enriched W from subducting crust into a mantle wedge source for the Nuvvuagittuq supracrustal rocks was suggested to generate high W concentrations in what is presumed to originally have been mantle-derived rocks [Touboul et al., 2014]. In that study, the geological setting for the highly altered rocks was identified using relative abundances of high field strength elements (HFSE). This approach is valid for both modern and some ancient lavas, as these elements have similar incompatibilities during mantle melting, but different mobilities in fluids. For example, Th is more mobile than Nb, leading to arc lavas with higher Th/Nb than MORB and ocean island basalts (OIB). On a plot of Nb/Yb versus Th/Yb, MORB and OIB are readily distinguishable from modern arc rocks (Figure 9a). However, on this discrimination diagram, the Schapenburg komatiites plot within the field defined by MORB and OIB.

Another way to identify a convergent margin origin for a lava is to compare the abundances of a highly mobile element, such as Ba, with those of the much less mobile HFSE and REE, such as Nb and La [Jenner et al., 2009]. In the case of the Nuvvuagittuq rocks, there are good correlations between W/Ba and Ba, consistent with fluid mobilization. The Schapenburg komatiites, however, plot on the MORB-OIB array in a Ba/La versus Ba/Nb diagram (Figure 9b). Finally, the Schapenburg komatiites are characterized by positive Nb anomalies ($\text{Nb}/\text{Nb}^* = 1.21 \pm 0.03$), typical of other uncontaminated, plume-derived komatiites [e.g., Puchtel et al., 1998], and in stark contrast to lavas produced in a subduction zone environment, which are characterized by strongly negative Nb anomalies. Collectively, these trace element systematics indicate that the W enrichment observed in the Schapenburg komatiites does not derive from permeating subduction-related fluids.

The high W concentrations also could reflect a high concentration of W in the mantle source of the komatiites resulting from the incorporation of recycled, early-formed crust. This possibility has the advantage that, if the crust formed sufficiently early, its projected low Hf/W (and Sm/Nd) would lead to depletions in ^{182}W (and ^{142}Nd), compared to ambient mantle. This is consistent with the isotopic compositions of the komatiites. However, enrichment in W resulting from crustal recycling would also lead to considerable enrichments

degrees of partial melting of mantle with W abundances similar to BSE (i.e., ~ 13 ppb). Ratios of W/Th and W/U, for example, range from 10 to 13 and 32 to 63, respectively (Figure 3), which are ~ 100 and ~ 75 times higher than those typical of mid-ocean ridge basalts (MORB), despite the similar incompatibility of U, Th, and W during crystal-liquid fractionation processes [e.g., Newsom et al., 1996; Arevalo and McDonough, 2008; König et al., 2011]. This indicates that W concentrations in the Schapenburg komatiites were not controlled solely by magmatic processes initiating in a portion of the mantle with BSE-like W abundances.

One possible way to explain the high W abundances is that the Schapenburg komatiites were generated in a subduction zone environment, as has been suggested for some other BGB komatiites (e.g., 3.48 Ga Komati Formation komatiites) [Grove and Parman, 2004]. Enrichments of W, relative to Th and U, have been reported for island arc lavas, and have been interpreted to reflect

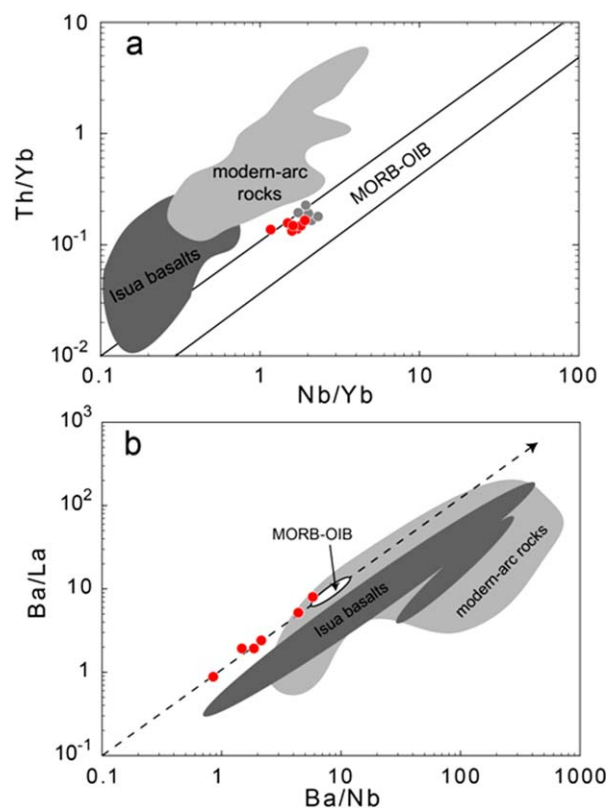


Figure 9. Plots of (a) Th/Yb versus Nb/Yb and (b) Ba/La versus Ba/Nb. Trace element data for the Schapenburg komatiites are from this study (red symbols) and Puchtel *et al.* [2009] (gray symbols). The light gray field, dark gray field, and open fields represent modern arc-derived rocks, basalts from the Isua GB, and MORB+OIB, respectively, as compiled by Jenner *et al.* [2009, and references therein], König *et al.* [2008, 2010], and König and Schuth [2011].

ized by a unique combination of short-lived and long-lived isotope features, as well as unusual HSE systematics. It is unknown whether some or most of these characteristics were established by a single common process, or a series of different processes. As the shortest lived system, the negative ^{182}W anomaly likely provides a record of the earliest event to have affected the mantle source of the Schapenburg komatiites. Here we review those ancient processes that could have led to negative ^{182}W isotope anomalies in terrestrial mantle sources. These include: (1) a contribution of W from core-derived materials, (2) an overabundance of late accreted materials relative to those present in the BSE, and (3) in situ decay of ^{182}Hf in a mantle reservoir with lower Hf/W than the ambient BSE. We consider these processes in turn below.

5.2.1. Core-Mantle Interaction

The addition of outer core metal to a deep mantle source will transfer a negative ^{182}W anomaly to the mantle if the bulk Earth has a chondritic $^{182}\text{W}/^{184}\text{W}$ ratio, i.e., $\mu^{182}\text{W} = -200$ [e.g., Scherstén *et al.*, 2004]. Mass balance calculations, using the abundance estimates of 13 ppb W for the BSE [Avalo and McDonough, 2008; König *et al.*, 2011] and 590 ppb W for the core [McDonough, 2004], require the core to have a $\mu^{182}\text{W}$ of ~ -220 to balance the more radiogenic isotopic composition of the mantle ($\mu^{182}\text{W} = 0$). Addition of core metal to a mantle domain would, therefore, lead to a decrease in the $\mu^{182}\text{W}$ value of that mantle domain. A mass contribution of $\sim 2\%$ of core metal to the mantle source of the Schapenburg komatiites would produce the necessary negative ^{182}W anomaly of -8 ppm. However, the addition of core metal would also lead to a marked increase in the abundances of HSE in that source. For example, a 2% addition of core metal to the ambient mantle, assuming that no inner core formation had occurred by the time of Schapenburg komatiite formation, would lead to Pt and Pd abundances well over 50 ppb. Such high abundances are inconsistent with the Pt and Pd abundances of 2.12 ± 0.36 and 2.15 ± 0.40 ppb, respectively, estimated

in other incompatible trace elements, such as U, Th, and LREE, which is not consistent with the low komatiite-like abundances measured in the Schapenburg komatiites.

Finally, the high W concentrations could reflect localized remobilization by hydrothermal alteration during emplacement, or accompanying thermal metamorphism affecting these rocks. However, all Schapenburg komatiites analyzed have uniform $\mu^{182}\text{W}$ values. This would be an unlikely outcome of variable alteration or metamorphic disturbance that would have affected olivine cumulate and spinifex-textured lavas in different ways, unless the fluid that transported the W had the same ^{182}W isotopic composition as the pristine komatiites. This would probably only occur if the fluids equilibrated with, or originated from rocks that were ultimately derived from the same mantle source as the komatiites themselves. Because of our inability to explain the W abundances in any other way, we conclude that this is the most likely cause for the high W abundances. Consequently, we interpret the ^{182}W isotopic composition of the Schapenburg komatiites to reflect the composition of their mantle source.

5.2. Origin of the Negative ^{182}W and ^{142}Nd Anomalies

The Schapenburg komatiites are character-

for the Schapenburg mantle source in this study. Moreover, because metal-silicate interaction would have no effect on the lithophile Sm-Nd isotope systems, the negative ^{142}Nd anomalies of the Schapenburg komatiites can be the result only of silicate-silicate fractionation processes while ^{146}Sm was still extant. Thus, a process in addition to core-mantle interaction would be needed to generate the observed negative anomalies for both isotope systems.

5.2.2. Disproportional Late Accretion

If late accreted materials were not instantaneously mixed and homogenized throughout the mantle, as seems likely, then portions of the mantle would be expected to initially have excesses and deficits of late accreted materials, compared to the average amount required to accommodate the HSE budget of the BSE [e.g., Willbold *et al.*, 2011, 2015]. The observed 8 ppm deficit in ^{182}W in the Schapenburg komatiites would be obtained in a mantle domain to which 1.4–1.8 times more late accreted materials, with chondritic W isotopic compositions, were added, relative to the present-day BSE. Such an excess of late accreted materials would also lead to proportionally higher HSE contents than BSE estimates, which is inconsistent with the strong depletion of HSE inferred for the source of the Schapenburg komatiites. Excess late accretionary component in the Schapenburg mantle domain further would have had negligible effect on the $^{142}\text{Nd}/^{144}\text{Nd}$ systematics because of the limited amount of added mass and the relatively low abundances of Sm and Nd in late accreted materials. As with the core interaction scenario, an additional process would be needed to explain the negative ^{142}Nd anomaly in the Schapenburg komatiite magma.

5.2.3. In Situ ^{182}Hf Decay in Incompatible Element-Enriched Mantle

Magmatic processes, such as partial melting of silicate rocks and crystallization of silicate liquids, lead to low Hf/W and low Sm/Nd in the liquids given the more incompatible nature of W and Nd compared to Hf and Sm [Newsom and Palme, 1984; Newsom *et al.*, 1996; Righter and Shearer, 2003; Salters and Longhi, 1999]. An early-formed, incompatible element-enriched mantle domain, or early crust, therefore, would evolve to deficits in both ^{182}W and ^{142}Nd compared to the BSE. As the Schapenburg komatiite source shows no evidence of enrichment by recycled crust (see section 5.1), we focus on intra-mantle processes that could lead to the isotopic characteristics of the komatiites. Deficits in ^{182}W place stronger constraints on the timing of early mantle processing than do deficits in ^{142}Nd because the half-life of ^{182}Hf is shorter than that of ^{146}Sm by about an order of magnitude. Since most ^{182}Hf has decayed away within the first 50 Ma of the start of Solar System history, ^{182}W heterogeneity caused by intra-mantle fractionation processes must have occurred within that short and early time window. In section 5.4, we model the evolution of a mantle source for the Schapenburg komatiites that was enriched in incompatible elements very early in Earth's history as a result of fractionation in a primordial magma ocean.

5.3. Constraints Provided by ^{143}Nd and ^{176}Hf

The long-lived ^{147}Sm - ^{143}Nd ($t_{1/2} = 106$ Ga) and ^{176}Lu - ^{176}Hf ($t_{1/2} = 37$ Ga) systems also would have been affected by early fractionation events in the silicate Earth. The fractionation of the Sm/Nd ratio required to generate depletion in ^{142}Nd would also have led to depletion in ^{143}Nd , yet the initial $\epsilon^{143}\text{Nd}$ value for the Schapenburg komatiite source is enriched relative to chondrites, and broadly consistent with estimates for the contemporary DMM. The positive initial $\epsilon^{143}\text{Nd}$ value is, therefore, in apparent conflict with the two short-lived isotope systems, under the common assumptions about the initially chondritic nature of the mantle. The comparison of the ^{146}Sm - ^{142}Nd and ^{147}Sm - ^{143}Nd systems is important here because both systems involve the same parent and daughter elements. The observed apparent discrepancy between the ^{142}Nd -depleted and ^{143}Nd -enriched compositions means that the decoupling of the two systems cannot be explained by a mineral structure-driven change in relative incompatibility of the two elements, such as can occur with changes in depth of melting within the mantle. Nor can it be explained by post-emplacment processes, such as hydrothermal alteration or metamorphism. This is because of the consistently uniform initial $\epsilon^{143}\text{Nd}$ values in all studied komatiite samples, and the magmatic nature of the Sm and Nd variations in the lavas, indicating no significant disturbance of the Sm-Nd isotope systematics since the time of komatiite emplacement. The seemingly conflicting initial ^{142}Nd - ^{143}Nd compositions potentially can be reconciled by calling on a later melt depletion event, most likely after ^{182}Hf was no longer extant and ^{146}Sm was greatly diminished, which could have led to a substantial increase in Sm/Nd, which in turn would have caused more rapid ingrowth of radiogenic ^{143}Nd .

The Lu/Hf ratio would also have been affected by silicate fractionation in a manner similar to the Sm/Nd ratio, if the fractionation process occurred at comparatively low, upper mantle pressures. In this scenario,

however, both the $^{176}\text{Hf}/^{177}\text{Hf}$ and the $^{143}\text{Nd}/^{144}\text{Nd}$ compositions of the Schapenburg komatiite source should have evolved along the terrestrial array (or the DMM curve), rather than to the observed enrichment in ^{176}Hf relative to ^{143}Nd , causing the Schapenburg komatiites to plot off the terrestrial array toward excesses in ^{176}Hf (Figure 8). One way to account for this incongruity, or decoupling, between Hf and Nd isotope compositions is by envisioning an initial fractionation event occurring at high pressures and temperatures, at depths between 700 and 2900 km. Under these conditions, Mg-perovskite and Ca-perovskite are the stable mantle phases [e.g., Ito *et al.*, 2004; Caro *et al.*, 2005]. Because most trace elements, except for Hf, are moderately to strongly incompatible in Mg-perovskite, but compatible in Ca-perovskite, especially the HREE [Corgne *et al.*, 2005], the presence of Ca-perovskite in the fractionating mineral assemblage of the lower mantle may result in stronger fractionation of Lu/Hf relative to Sm/Nd than observed under upper mantle conditions [e.g., Caro *et al.*, 2005; Rizo *et al.*, 2011; Puchtel *et al.*, 2013]. Fractionation of a mixed Mg-perovskite and Ca-perovskite mineral assemblage therefore would lead to more suprachondritic Lu/Hf relative to Sm/Nd in the mantle source, which in turn would have grown in an excess of ^{176}Hf compared to ^{143}Nd by the time of komatiite emplacement.

5.4. Three-Stage Model for the Formation of the Schapenburg Komatiite Source

The accretionary history of the Earth was undoubtedly complex, involving multiple stages of growth over a protracted period of time [e.g., Rubie *et al.*, 2011]. In the previous sections, we showed that constraints from trace elements and four radiogenic isotope systems on the source of the Schapenburg komatiites could be satisfied at a first-order level by core formation followed by mantle melting processes over protracted periods of time. These mantle processes include very early silicate fractionation in a magma ocean, while ^{182}W and ^{146}Sm were still alive, followed by a later episode of incompatible element depletion. In the following, we describe a quantitative model that can account for many of the geochemical characteristics of the Schapenburg komatiites. The model does not provide a unique solution to the evolutionary history of the precursor materials to the komatiites, but serves to elucidate the timing and types of processes necessary to ultimately result in the ^{182}W - ^{142}Nd - ^{143}Nd - ^{176}Hf isotopic compositions measured for these komatiites.

For this model, we envision three stages of chemical evolution of a mantle domain that, together, lead to the formation of the Schapenburg komatiite source with the chemical and isotopic characteristics documented in this study. To explore effects on the Hf-W, Sm-Nd, and Lu-Hf isotope systems during these stages, we use published partition coefficients for the elements in question in the appropriate mantle phases. Table 7 provides the parameters and time intervals used for each evolutionary stage. Evolution diagrams for each of the four isotope systems modeled are shown in Figure 10.

Stage 1 extends for 31 Ma from the time of Solar System formation at 4568–4537 Ma as the proto Earth grows, while maintaining average chondritic Hf/W, Sm/Nd, and Lu/Hf ratios. At 4537 Ma, Stage 2 begins, as the Earth differentiates to form a core and a mantle. A lower mantle magma ocean instantaneously undergoes high-pressure removal of Mg-perovskite and Ca-perovskite, resulting from 10% fractional crystallization. The removal of these mineral phases leads to the creation of a mantle domain with subchondritic Hf/W and Sm/Nd, but slightly suprachondritic Lu/Hf. This domain evolves for an additional 510 Ma, until 4027 Ma, whereupon mantle convection has transported the domain into the upper mantle. At the beginning of Stage 3 at 4027 Ma, this domain undergoes 5% batch melting at comparatively low pressures, and the resulting residue evolves to suprachondritic Hf/W and Sm/Nd ratios; the Lu/Hf ratio, which already was suprachondritic, becomes even more suprachondritic. It is this residue that melts at 3550 Ma to produce the Schapenburg komatiites.

Several aspects of this model require justification. First, Stage 2 of the model is initiated by a single-stage core separation event for the proto Earth, 31 Myr after Solar System formation. A single core separation event is not consistent with dynamical models for the early Solar System which hold that the rocky planets were built through energetic stages of oligarchic and finally giant impact growth [e.g., Jacobson and Walsh, 2015]. Major growth events likely led to repeated partial or complete melting of the proto Earth, protracted growth of the core, and some level of repeated chemical and isotopic equilibrations between metals sinking to form cores, and silicates [e.g., Rubie *et al.*, 2011; Nimmo and Kleine, 2015]. The Hf-W isotopic system, whose mantle evolution reflects changes in Hf/W resulting from both metal-silicate differentiation and silicate-silicate fractionation, must have undergone complex isotopic evolution over the first several tens of Ma of Earth history [e.g., Halliday, 2004]. Despite this complexity, the W isotopic composition of the mantle

Table 7. Parameters Used to Model Chemical and Isotopic Evolution of the Source of the Schapenburg Komatiites^a

Stage 1: Earliest Earth Accretion					
¹⁸⁰ Hf/ ¹⁸⁴ W	1.30				
¹⁴⁷ Sm/ ¹⁴⁴ Nd	0.1960				
¹⁷⁶ Lu/ ¹⁷⁷ Hf	0.03360				
Stage 2: Core Segregation and Lower Mantle Melting (F = 0.9) at 4537 Ma					
	D _{Hf}	D _W	D _{Lu}	D _{Sm}	D _{Nd}
Mg-perovskite	1.8	0.45	0.73	0.07	0.02
Ca-perovskite	2.1	0.27	11	20	16
¹⁸⁰ Hf/ ¹⁸⁴ W	20.81				
¹⁴⁷ Sm/ ¹⁴⁴ Nd	0.1910				
¹⁷⁶ Lu/ ¹⁷⁷ Hf	0.0357				
Stage 3: Upper Mantle Melting (F = 0.05) at 4027 Ma					
	D _{Hf}	D _W	D _{Lu}	D _{Sm}	D _{Nd}
Olivine	0.01	0	0.017	0.00017	0.00003
Orthopyroxene	0.08	0.011	0.13	0.011	0.004
Clinopyroxene	0.5	0.10	0.425	0.47	0.28
Garnet	0.8		10	0.33	0.008
¹⁴⁷ Sm/ ¹⁴⁴ Nd	0.2380				
¹⁷⁶ Lu/ ¹⁷⁷ Hf	0.0492				
Melting Komatiite Source (F = 0.20) at 3550 Ma					
	D _{Hf}		D _{Lu}	D _{Sm}	D _{Nd}
Olivine	0.01		0.017	0.00017	0.00003
Orthopyroxene	0.08		0.13	0.011	0.0034
Clinopyroxene	0.50		0.425	0.331	0.140
Pyrope garnet	1.2		3.79	0.830	0.363
¹⁴⁷ Sm/ ¹⁴⁴ Nd	0.2075				
¹⁷⁶ Lu/ ¹⁷⁷ Hf	0.0355				
FC of Pyrope Garnet (F = 0.15) From the Komatiitic Magma at 3550 Ma					
	D _{Hf}		D _{Lu}	D _{Sm}	D _{Nd}
Pyrope garnet	1.2		3.79	0.830	0.363
¹⁴⁷ Sm/ ¹⁴⁴ Nd	0.1923				
¹⁷⁶ Lu/ ¹⁷⁷ Hf	0.0233				

^aNote: lower mantle assemblage: 95% Mg-perovskite + 5% Ca-perovskite. Upper mantle assemblage for Stage 2: 60% Ol + 20% Opx + 20% Cpx. Upper mantle komatiite source assemblage: 80% Ol + 10% Opx + 5% Cpx + 5% Gar. Partition coefficients for olivine, clinopyroxene, orthopyroxene, garnet, and pyrope garnet are from Green [1994]; values for Mg-perovskite and Ca-perovskite are from *Corgne et al.* [2005]. Partition coefficients for W in Mg-perovskite and Ca-perovskite are calculated using the lattice strain model of *Corgne et al.* [2005]. F = fraction of melting.

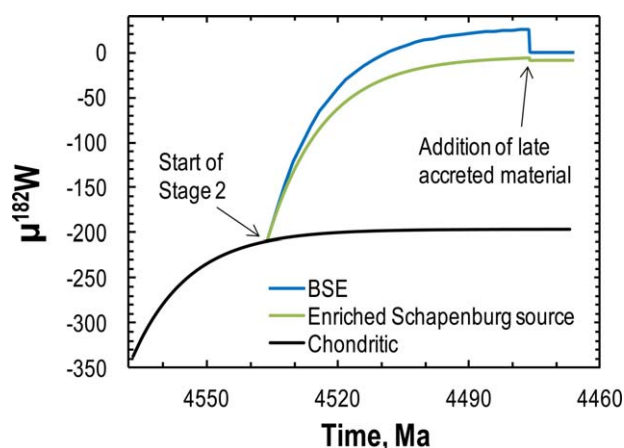


Figure 10. Isotopic evolution of ¹⁸²W during early Earth history, calculated using three sets of conditions. Parameters are given in Table 7. Chondritic evolution represents Earth's source materials and bulk composition, and provides the earliest, Stage 1, evolution to a mantle source from which the Schapenburg komatiites were ultimately derived. At the beginning of Stage 2, at 4537 Ma, Hf/W was fractionated during core formation into Bulk Silicate Earth (BSE) and a melt-enriched source, likely components of a magma ocean. After core segregation and some additional period of ingrowth of ¹⁸²W, less radiogenic late accreted material was added to both BSE and the enriched source.

today, combined with an estimated ¹⁸⁰Hf/¹⁸⁴W for the BSE of ~24, gives a two stage model core formation age of ~30 Ma after Solar System formation [e.g., *Yin et al.*, 2002; *Kleine et al.*, 2009]. Thus, the interval we use for the termination of Stage 1 chondritic growth is consistent with the time-averaged growth trajectory of ¹⁸²W in the BSE. It is the slightly lower Hf/W ratio, relative to the BSE, used in Stage 2 that establishes the ¹⁸²W depletion carried through Stages 2 and 3. For the present model, we used Solar System initial ¹⁸²W/¹⁸⁴W and ¹⁸²Hf/¹⁸⁰Hf ratios of 0.864477 and 0.000102, respectively [*Krujer et al.*, 2014].

As discussed in section 4.2 and later in section 5.5, the Schapenburg komatiites were likely derived from a mantle source that had received only about a third of the late accretionary component present in the BSE today. A deficit in late accreted components in such a mantle domain

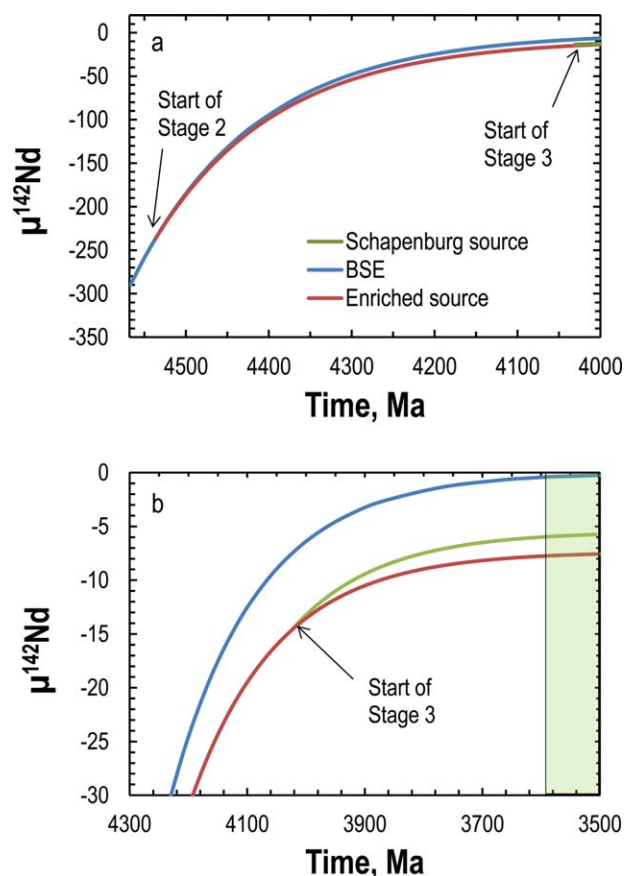


Figure 11. Isotopic evolution of ^{142}Nd from Solar System formation until the time of melting to form the Schapenburg komatiites (green field). Calculation parameters for the models are given in Table 7. (a) Early fractionation of Sm/Nd at the beginning of Stage 2, at 4537 Ma, during which fractional crystallization of the BSE reservoir creates an enriched source. At 4027 Ma, the enriched reservoir was melt depleted. (b) Detail of the fractionation at 4027 Ma, which shows the separate evolution of the enriched source formed in Stage 2 and the melt-depleted source from which the Schapenburg komatiites were ultimately derived.

2015]. This value serves as a good estimate for the contemporary ambient mantle. Combining these μ values, -3 and $+26$, provides the offset of $29 \mu^{182}\text{W}$ units between the ambient mantle and the Schapenburg mantle source that would have been generated by the end of Stage 2 if no late accreted material was added to either. The values of $\mu^{182}\text{W} = +26$ for the contemporary BSE and -3 for the Schapenburg source, are, therefore, the goals of the Stage 2 modeling (Figure 11a). At some time during Stage 2, 0.12% of late accreted mass was added to the source of the Schapenburg komatiites to bring its $\mu^{182}\text{W}$ down to the measured value of -8.5 ; similarly, 0.5% of late accreted mass was added to the ambient mantle to bring its $\mu^{182}\text{W}$ down to 0. Our model komatiite source yields a $\mu^{182}\text{W}$ value of -4.0 at the end of Stage 2 (and Stage 3), which is a good fit to the projected pre late accretionary $\mu^{182}\text{W}$ value of -3 .

Modeling the ^{146}Sm - ^{142}Nd system also requires some assumptions. It was first noted by Boyet and Carlson [2005] that the $^{142}\text{Nd}/^{144}\text{Nd}$ ratio of the BSE is 10–20 ppm higher than most bulk chondrites. This has been explained by one of three processes: (1) creation of an early enriched reservoir with subchondritic Sm/Nd that was subsequently permanently removed to the lower mantle, leaving the bulk of the mantle with suprachondritic Sm/Nd that gradually evolved to the observed suprachondritic $^{142}\text{Nd}/^{144}\text{Nd}$ [Boyet and Carlson, 2005], (2) removal by collisional erosion of chemically evolved crusts, with subchondritic Sm/Nd, from the planetary building blocks of Earth, eventually resulting in a BSE with suprachondritic Sm/Nd, that again, gradually evolved to the observed apparently suprachondritic $^{142}\text{Nd}/^{144}\text{Nd}$ [O'Neill and Palme, 2008], and (3) construction of the Earth from building blocks that were enriched in nuclides produced by s-process

would not only affect its HSE abundances, but also its Hf/W ratio, and, hence, the magnitude of ^{182}W ingrowth. This mantle domain must have been isolated from the BSE while ^{182}Hf was extant, but prior to the dominant phase of late accretion, which likely occurred after 4511 Ma, the minimum age for the Moon-forming impact [Touboul *et al.*, 2015]. How would the $\mu^{182}\text{W}$ of such a domain that was missing part of its late accretionary component compare to the ambient mantle at any given time? This domain would be more radiogenic than ambient mantle, because it would contain less of the late accreted, low $\mu^{182}\text{W}$ component. To quantify the ^{182}W isotopic difference between the Schapenburg mantle source and the contemporary ambient mantle, it is, therefore, necessary to remove the isotopic effects of late accretion from both. Mathematical removal of a mass fraction of approximately 0.12% of chondritic material from contemporary ambient mantle to produce the Schapenburg source (i.e., removal of the amount that would have provided it with 29% of the HSE present in the BSE today), would increase the $\mu^{182}\text{W}$ value of the source from its present-day measured value of -8.5 to ~ -3 . Removal of the entire 0.5% of late accreted mass from the present mantle would increase its $\mu^{182}\text{W}$ value from 0 to $\sim +26$, a value that is similar to the isotopic composition of the HSE-poor lunar mantle [Kruijer *et al.*, 2015; Touboul *et al.*,

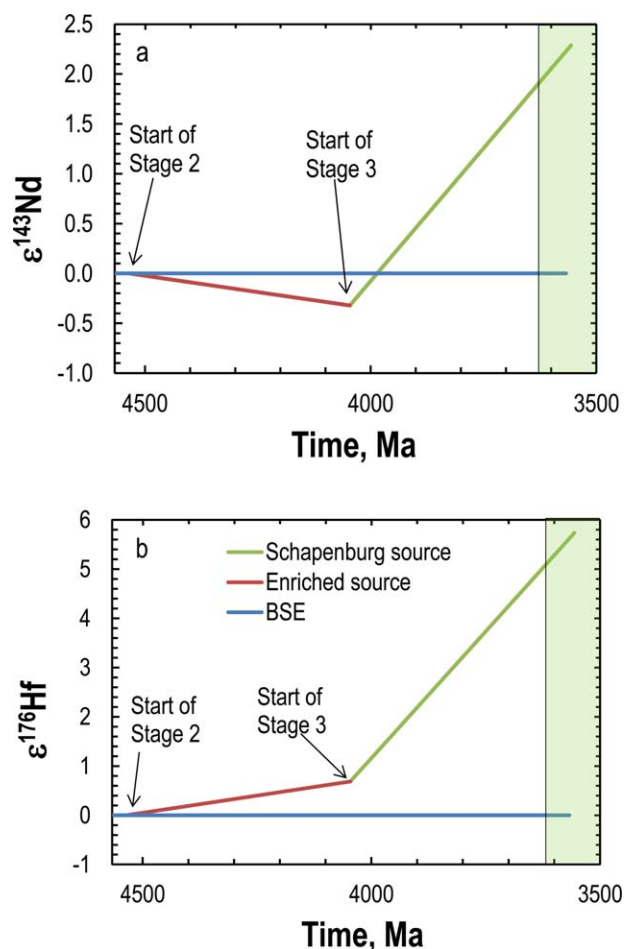


Figure 12. Isotopic evolution of (a) $\epsilon^{143}\text{Nd}$ and $\epsilon^{176}\text{Hf}$ from the beginning of the Solar System to the time at which the Schapenberg komatiites were formed (green field). Calculation parameters for the models are given in Table 7. (a) Fractional crystallization of BSE at high pressure at the start of Stage 2 retarded the growth of ^{143}Nd (and ^{142}Nd , Figure 11). A subsequent melt depletion event drove $\epsilon^{143}\text{Nd}$ to the positive values measured in the source of the Schapenberg komatiites. (b) Both high-pressure fractional crystallization of BSE and lower pressure melt depletion allowed faster ingrowth of radiogenic Hf relative to BSE. Contrasting distribution coefficients for Ca-perovskite, compared to clinopyroxene, result in different growth trajectories for radiogenic ^{143}Nd and ^{176}Hf during Stage 2.

because at high pressure in a largely Mg-perovskite-dominated source, Hf is more compatible than Lu. Consequently, the initial stage of fractional crystallization of a lower mantle magma ocean results in a fractionated liquid with slightly suprachondritic Lu/Hf, which at the same time leads to normal to subchondritic Sm/Nd (Table 7). This allows ^{176}Hf to grow in proportionally faster than ^{143}Nd during Stage 2 (Figures 12a and 12b). Subsequent melt removal at lower pressure starts off Stage 3 and results in proportionally similar growth of ^{143}Nd and ^{176}Hf in the residue during the final stage of evolution. The end of Stage 3 of the model source is characterized by $\epsilon^{143}\text{Nd}$ and $\epsilon^{176}\text{Hf}$ values of +2.2 and +5.7, respectively, which are good fits to the initial $\epsilon^{143}\text{Nd}$ and $\epsilon^{176}\text{Hf}$ values of the Schapenberg komatiites of +2.4 and +5.7.

Based on the modeling results for Stage 3, the Schapenberg komatiite mantle source contained 0.0653 ppm Lu, 0.188 ppm Hf, 0.268 ppm Sm, and 0.696 ppm Nd ($^{147}\text{Sm}/^{144}\text{Nd} = 0.233$, $^{176}\text{Lu}/^{177}\text{Hf} = 0.0493$). Using regressions of Sm, Nd, Lu, and Hf versus MgO abundances for the suite of the Schapenberg komatiite samples studied, and applying the emplaced lava MgO content of 27 wt.% [Puchtel et al., 2009], the emplaced komatiite lava is estimated to have contained 0.103 ppm Lu, 0.626 ppm Hf, 1.12 ppm Sm, and 3.52 ppm Nd ($^{147}\text{Sm}/^{144}\text{Nd} = 0.192$, $^{176}\text{Lu}/^{177}\text{Hf} = 0.0234$). We modeled the generation of the Schapenberg

nucleosynthesis, including ^{142}Nd [Gannoun et al., 2011; Burkhardt et al., 2016; Fukai and Yokoyama, 2016]. Evolution models for ^{142}Nd in Earth's mantle are strongly affected by the process chosen. Both of the first two scenarios require a BSE with Sm/Nd that is suprachondritic. The third process allows the assumption of chondritic Sm/Nd for the BSE. Because recent studies of terrestrial materials have shown enrichments/depletions in other s-process isotopes (^{148}Nd , ^{150}Nd) that correspond to the enrichment in ^{142}Nd [Burkhardt et al., 2016; Fukai and Yokoyama, 2016], we base our model on the assumption of a BSE with chondritic $^{147}\text{Sm}/^{144}\text{Nd} = 0.196$ [Bouvier et al., 2008]. We calculate an initial $^{142}\text{Nd}/^{144}\text{Nd}$ for Earth of 1.141503, using the chondritic Sm/Nd ratio, together with an assumption of a Solar System initial $^{146}\text{Sm}/^{144}\text{Sm} = 0.0083$ [Marks et al., 2014] and modern mantle $^{142}\text{Nd}/^{144}\text{Nd} = 1.141837$ (the average of our analyses of the AMES Nd standard). Our model komatiite source yields a $\mu^{142}\text{Nd}$ value of -5.8 at the end of Stage 3, which is a good fit to the observed $\mu^{142}\text{Nd}$ value of -5.0 ± 2.8 .

The long-lived ^{147}Sm - ^{143}Nd and ^{176}Lu - ^{176}Hf isotopic systems lead to some peculiarities in the model. The model requires partial crystallization of a magma ocean within the stability field of Mg-perovskite and Ca-perovskite (at depths >700 km) at 4537 Ma. High-pressure processing allows $\epsilon^{176}\text{Hf}$ of the Schapenberg source to evolve during Stage 2 to more radiogenic values than the terrestrial $\epsilon^{143}\text{Nd}$ versus $\epsilon^{176}\text{Hf}$ array (Figure 8). This is achieved

emplaced komatiite lava from the mantle source with the initial concentration parameters above, using partition coefficients for these elements from Green [1994].

The model consists of 20% batch melting of a peridotitic source (80% Ol + 10% Opx + 5% Cpx + 5% Gar) to produce an initial komatiite magma with 0.168 ppm Lu, 0.670 ppm Hf, 1.08 ppm Sm, and 3.16 ppm Nd ($^{147}\text{Sm}/^{144}\text{Nd} = 0.208$, $^{176}\text{Lu}/^{177}\text{Hf} = 0.0355$). During ascent, 15% fractional crystallization of pyrope garnet from the Al-undepleted komatiite magma leads to formation of an Al-depleted komatiite melt with 0.106 ppm Lu, 0.648 ppm Hf, 1.11 ppm Sm, and 3.50 ppm Nd ($^{147}\text{Sm}/^{144}\text{Nd} = 0.192$, $^{176}\text{Lu}/^{177}\text{Hf} = 0.0233$). These concentrations are in good agreement with the calculated composition of the emplaced Schapenburg komatiite lava.

5.5. ^{187}Re - ^{187}Os Systematics

As noted above, ^{187}Os also shows a 3.7% enrichment compared to chondritic mantle evolution models. This isotopic system, however, is problematic to quantitatively model for the processes discussed above, because of the lack of high-pressure partition coefficients for Re and Os in dominantly silicate systems. More importantly, the HSE projected for the Schapenburg source are estimated to have been in nonchondritic relative abundances [e.g., Puchtel *et al.*, 2009, and this study], implying that assumptions about an initially chondritic source modified by crystal-liquid fractionation processes is probably not valid for this system. In general, Re is moderately incompatible in silicate systems, while Os remains compatible. Consequently, incompatible element-enriched fractionates from a magma ocean would be expected to be characterized by enrichments in Re/Os and evolve to enrichments in ^{187}Os over the ~ 500 Myr of evolution allotted to Stage 2 of the present model. The depletion event that initiates Stage 3 would likely have lowered the Re/Os ratio to subchondritic. Whether or not the next ~ 400 Myr of evolution would offset the growth in ^{187}Os created by the second stage cannot be modeled to a sufficient level of precision. We, therefore, conclude that the Os isotopic characteristics of these komatiites cannot be quantified in a useful manner at this time.

6. Conclusions

The 3.55 Ga komatiites from the Schapenburg Greenstone Remnant in South Africa are some of the oldest lavas on Earth that can be unambiguously classified as belonging to this class of high-MgO volcanic rocks. These komatiites, which preserve many of their original textural, mineralogical, and chemical features, have a unique combination of trace element abundances and isotopic compositions that place strong constraints on their origin.

The Schapenburg komatiites show coupled depletions, relative to the modern mantle, in ^{142}Nd and ^{182}W ($\mu^{142}\text{Nd} = -5.0 \pm 2.8$, $\mu^{182}\text{W} = -8.4 \pm 4.5$, 2SD), the decay products of the short-lived ^{146}Sm and ^{182}Hf nuclides, respectively. The deficit in ^{182}W is inconsistent with lack of late accreted material in their mantle source, as such a source would be expected to have an excess in ^{182}W . These isotopic compositions instead require derivation from mantle that was enriched in incompatible elements ~ 30 Ma after Solar System formation. Early Hadean contributors to this mantle domain could include high-pressure fractionates from a magma ocean.

By contrast, the long-lived, lithophile, refractory Sm-Nd and Lu-Hf isotope systems ($\epsilon^{143}\text{Nd} = +2.4 \pm 0.1$, $\epsilon^{176}\text{Hf} = +5.7 \pm 0.3$, 2SD) show that the komatiite mantle source underwent additional processing after the early Hadean, including melt depletion at lower pressures. The primary komatiite magma formed via 20% batch melting of this trace element-depleted peridotite mantle source, followed by 15% fractional crystallization of pyrope garnet.

Early-formed ^{182}W and ^{142}Nd anomalies persisted in the Schapenburg mantle source throughout the Hadean and early Archean, despite later planetary accretion, melting, and convection. Some other komatiites, including those from the early Archean Barberton Greenstone Belt [Puchtel *et al.*, 2014] and the 2.8 Ga Kostomuksha komatiites [Touboul *et al.*, 2012], also were sourced from mantle domains with compositionally diverse, but extraordinarily ancient isotopic heterogeneities. The preservation of these anomalous domains reflects their stability during even the earliest parts of Earth's history.

Acknowledgments

This work was supported by NSF-CSEDI grant EAR 1265169 to RJW, NSF Petrology and Geochemistry grant EAR 1447174 to ISP, ANR grant ANR-10-BLANC-0603 M&Ms – Mantle Melting – Measurements, Models, Mechanisms to JBT, and NSF-IF grant EAR 0549300, which provided partial support for the Triton mass-spectrometer used for most of the measurements in this study. We are grateful to Carl Anhaeusser for providing the drill core samples, to Valentina Puchtel and Richard Ash for help with preparation of samples and ICP-MS measurements at the IGL and PL, and to Philippe Telouk for maintenance of the MC-ICP-MS in Lyon. Detailed constructive reviews by Claude Herzberg, Carsten Münker, and an anonymous reviewer helped substantially improve the original version of the manuscript. We thank Thorsten Becker for editorial handling of the manuscript in a most timely and efficient manner. The data that support the conclusions presented in this manuscript are either provided in the data tables and figures or is properly cited and referred to in the reference list.

References

- Anhaeusser, C. R. (1983), The geology of the Schapenburg greenstone remnant and surrounding Archaean granitic terrane south of Badplaas, Eastern Transvaal, Contributions to the Geology of the Barberton Mountain Land. C. R. Anhaeusser, *Spec. Publ. Geol. Soc. S. Afr.*, 9, 31–44.
- Anhaeusser, C. R. (1991), Schapenburg greenstone remnant, in *Two Cratons and an Orogen—Excursion Guidebook and Review Articles for a Field Workshop Through Selected Archaean Terranes of Swaziland, South Africa and Zimbabwe*, edited by L. D. Ashwal, pp. 107–115, Univ. of the Witwatersrand, Johannesburg, South Africa.
- Anhaeusser, C. R., and L. J. Robb (1980), Regional and detailed field and geochemical studies of Archaean trondhjemitic gneisses, migmatites and greenstone xenoliths in the southern part of the Barberton Mountain Land, South Africa, *Precambrian Res.*, 11(3–4), 373–397.
- Arevalo, R., and W. F. McDonough (2008), Tungsten geochemistry and implications for understanding the Earth's interior, *Earth Planet. Sci. Lett.*, 272(3–4), 656–665.
- Barnes, S.-J., A. J. Naldrett, and M. P. Gorton (1985), The origin of the fractionation of platinum-group elements in terrestrial magmas, *Chem. Geol.*, 53(3–4), 303–323.
- Becker, H., M. F. Horan, R. J. Walker, S. Gao, J.-P. Lorand, and R. L. Rudnick (2006), Highly siderophile element composition of the Earth's primitive upper mantle: Constraints from new data on peridotite massifs and xenoliths, *Geochim. Cosmochim. Acta*, 70(17), 4528–4550.
- Bennett, V. C. (2003), Compositional Evolution of the Mantle, in *Treatise on Geochemistry*, pp. 493–519, Pergamon, Oxford, U. K.
- Birck, J. L., M. Roy-Barman, and F. Capman (1997), Re-Os isotopic measurements at the femtomole level in natural samples, *Geostand. NewsL.*, 20(1), 19–27.
- Blichert-Toft, J. (2001), On the Lu-Hf isotope geochemistry of silicate rocks, *Geostand. NewsL.*, 25(1), 41–56.
- Blichert-Toft, J., and F. Albarède (1997), The Lu-Hf isotope geochemistry of chondrites and the evolution of the mantle-crust system, *Earth Planet. Sci. Lett.*, 148(1–2), 243–258.
- Blichert-Toft, J., and I. S. Puchtel (2010), Depleted mantle sources through time: Evidence from Lu-Hf and Sm-Nd isotope systematics of Archean komatiites, *Earth Planet. Sci. Lett.*, 297(3–4), 598–606.
- Blichert-Toft, J., C. Chauvel, and F. Albarède (1997), Separation of Hf and Lu for high-precision isotope analysis of rock samples by magnetic sector multiple collector ICP-MS, *Contrib. Mineral. Petrol.*, 127(3), 248–260.
- Blichert-Toft, J., M. Boyet, P. Telouk, and F. Albarède (2002), ^{147}Sm - ^{143}Nd and ^{176}Lu - ^{176}Hf in eucrites and the differentiation of the HED parent body, *Earth Planet. Sci. Lett.*, 204(1–2), 167–181.
- Blichert-Toft, J., N. T. Arndt, and G. Gruau (2004), Hf isotopic measurements on Barberton komatiites: Effects of incomplete sample dissolution and importance for primary and secondary magmatic signatures, *Chem. Geol.*, 207(3–4), 261–275.
- Blichert-Toft, J., N. T. Arndt, A. Wilson, and G. Coetzee (2015), Hf and Nd isotope systematics of early Archean komatiites from surface sampling and ICDP drilling in the Barberton Greenstone Belt, South Africa, *Am. Mineral.*, 100(11–12), 2396–2411.
- Bouvier, A., J. D. Vervoort, and P. J. Patchett (2008), The Lu-Hf and Sm-Nd isotopic composition of CHUR: Constraints from unequilibrated chondrites and implications for the bulk composition of terrestrial planets, *Earth Planet. Sci. Lett.*, 273(1–2), 48–57.
- Boyet, M., and R. W. Carlson (2005), ^{142}Nd evidence for early (> 4.53 Ga) global differentiation of the silicate Earth, *Science*, 309(5734), 576–581.
- Burkhardt, C., L. E. Borg, G. A. Brennecke, Q. R. Shollenberger, N. Dauphas, and T. Kleine (2016), Meteoritic Nd isotope constraints on the origin and composition of the Earth, *Lunar Planet. Sci.*, XXXVII, Abstract 1908.
- Carlson, R. W., M. Boyet, and M. Horan (2007), Chondrite barium, neodymium, and samarium isotopic heterogeneity and early earth differentiation, *Science*, 316(5828), 1175–1178.
- Caro, G., B. Bourdon, B. J. Wood, and A. Corgne (2005), Trace-element fractionation in Hadean mantle generated by melt segregation from a magma ocean, *Nature*, 436(7048), 246–249.
- Chou, C.-L., D. M. Shaw, and J. H. Crocket (1983), Siderophile trace elements in the Earth's oceanic crust and upper mantle, *J. Geophys. Res.*, 88(S2), A507–A518.
- Cohen, A. S., and F. G. Waters (1996), Separation of osmium from geological materials by solvent extraction for analysis by thermal ionisation mass spectrometry, *Anal. Chim. Acta*, 332(2–3), 269–275.
- Corgne, A., C. Liebske, B. J. Wood, D. C. Rubie, and D. J. Frost (2005), Silicate perovskite-melt partitioning of trace elements and geochemical signature of a deep perovskitic reservoir, *Geochim. Cosmochim. Acta*, 69(2), 485–496.
- Creaser, R. A., D. A. Papanastassiou, and G. J. Wasserburg (1991), Negative thermal ion mass-spectrometry of osmium, rhenium, and iridium, *Geochim. Cosmochim. Acta*, 55(1), 397–401.
- Fukai, R., and T. Yokoyama (2016), Nucleosynthetic neodymium isotope anomalies in carbonaceous and ordinary chondrites, *Lunar Planet. Sci.*, XXXVII, Abstract 1298.
- Gannoun, A., M. Boyet, H. Rizo, and A. El Goresy (2011), ^{146}Sm - ^{142}Nd systematics measured in enstatite chondrites reveals a heterogeneous distribution of ^{142}Nd in the solar nebula, *Proc. Natl. Acad. Sci. U. S. A.*, 108(19), 7693–7697.
- Goldstein, S. L., R. K. O'Nions, and P. J. Hamilton (1984), A Sm-Nd isotopic study of atmospheric dusts and particulates from major river systems, *Earth Planet. Sci. Lett.*, 70(2), 221–236.
- Green, T. H. (1994), Experimental studies of trace-element partitioning applicable to igneous petrogenesis—Sedona 16 years later, *Chem. Geol.*, 117(1–4), 1–36.
- Grove, T. L., and S. W. Parman (2004), Thermal evolution of the Earth as recorded by komatiites, *Earth Planet. Sci. Lett.*, 219(3–4), 173–187.
- Halliday, A. N. (2004), Mixing, volatile loss and compositional change during impact-driven accretion of the Earth, *Nature*, 427(6974), 505–509.
- Hamilton, P. J., R. K. O'Nions, D. Bridgwater, and A. P. Nutman (1983), Sm-Nd studies of Archaean metasediments and metavolcanics from West Greenland and their implications for the Earth's early history, *Earth Planet. Sci. Lett.*, 62(2), 263–272.
- Hofmann, A. W. (1988), Chemical differentiation of the Earth: The relationship between mantle, continental crust and oceanic crust, *Earth Planet. Sci. Lett.*, 90(3), 297–314.
- Horan, M. F., R. J. Walker, J. W. Morgan, J. N. Grossman, and A. E. Rubin (2003), Highly siderophile elements in chondrites, *Chem. Geol.*, 196(1–4), 5–20.
- Ito, E., A. Kubo, T. Katsura, and M. J. Walter (2004), Melting experiments of mantle materials under lower mantle conditions with implications for magma ocean differentiation, *Phys. Earth Planet. Inter.*, 143, 397–406.
- Jacobsen, S. B., and G. J. Wasserburg (1980), Sm-Nd isotopic evolution of chondrites, *Earth Planet. Sci. Lett.*, 50(1), 139–155.
- Jacobson, S. A., and K. J. Walsh (2015), Earth and terrestrial planet formation, in *The Early Earth*, edited by J. Badro and M. J. Walter, pp. 49–70, John Wiley, Hoboken, N. J.

- Jahn, B. M., G. Gruau, and A. Y. Glikson (1982), Komatiites of the Onverwacht Group, South Africa: REE geochemistry, Sm-Nd age and mantle evolution, *Contrib. Mineral. Petrol.*, *80*(1), 25–40.
- Jenner, F. E., V. C. Bennett, A. P. Nutman, C. R. L. Friend, M. D. Norman, and G. Yaxley (2009), Evidence for subduction at 3.8 Ga: Geochemistry of arc-like metabasalts from the southern edge of the Isua Supracrustal Belt, *Chem. Geol.*, *261*(1–2), 82–97.
- Keays, R. R. (1995), The role of komatiitic and picritic magmatism and S-saturation in the formation of ore deposits, *Lithos*, *34*(1–3), 1–18.
- Kimura, K., R. S. Lewis, and S. Anders (1974), Distribution of gold and rhenium between nickel-iron and silicate melts; implications for abundance of siderophile elements on the earth and moon, *Geochim. Cosmochim. Acta*, *38*(5), 683–701.
- Kleine, T., K. Mezger, C. Münker, H. Palme, and A. Bischoff (2004a), ^{182}Hf - ^{182}W isotope systematics of chondrites, eucrites, and martian meteorites: Chronology of core formation and early mantle differentiation in Vesta and Mars, *Geochim. Cosmochim. Acta*, *68*(13), 2935–2946.
- Kleine, T., K. Mezger, H. Palme, and C. Münker (2004b), The W isotope evolution of the bulk silicate Earth: Constraints on the timing and mechanisms of core formation and accretion, *Earth Planet. Sci. Lett.*, *228*(1–2), 109–123.
- Kleine, T., M. Touboul, B. Bourdon, F. Nimmo, K. Mezger, H. Palme, S. B. Jacobsen, Q.-Z. Yin, and A. N. Halliday (2009), Hf-W chronology of the accretion and early evolution of asteroids and terrestrial planets, *Geochim. Cosmochim. Acta*, *73*(17), 5150–5188.
- König, S., and S. Schuth (2011), Deep melting of old subducted oceanic crust recorded by superchondritic Nb/Ta in modern island arc lavas, *Earth Planet. Sci. Lett.*, *301*(1–2), 265–274.
- König, S., C. Münker, S. Schuth, and D. Garbe-Schonberg (2008), Mobility of tungsten in subduction zones, *Earth Planet. Sci. Lett.*, *274*(1–2), 82–92.
- König, S., C. Münker, S. Schuth, A. Luguet, J. E. Hoffmann, and J. Kuduon (2010), Boninites as windows into trace element mobility in subduction zones, *Geochim. Cosmochim. Acta*, *74*(2), 684–704.
- König, S., C. Münker, S. Hohl, H. Paulick, A. R. Barth, M. Lagos, J. Pfander, and A. Büchl (2011), The Earth's tungsten budget during mantle melting and crust formation, *Geochim. Cosmochim. Acta*, *75*(8), 2119–2136.
- Kröner, A., E. Hegner, J. I. Wendt, and G. R. Byerly (1996), The oldest part of the Barberton granitoid-greenstone terrain, South Africa: Evidence for crust formation between 3.5 and 3.7 Ga, *Precambrian Res.*, *78*(1–3), 105–124.
- Kruijer, T. S., M. Touboul, M. Fischer-Gödde, K. R. Bermingham, R. J. Walker, and T. Kleine (2014), Protracted core formation and rapid accretion of protoplanets, *Science*, *344*(6188), 1150–1154.
- Kruijer, T. S., T. Kleine, M. Fischer-Gödde, and P. Sprung (2015), Lunar tungsten isotopic evidence for the late veneer, *Nature*, *520*(7548), 534–537.
- Lahaye, Y., N. T. Arndt, G. Byerly, C. Chauvel, S. Fourcade, and G. Gruau (1995), The influence of alteration on the trace-element and Nd isotopic compositions of komatiites, *Chem. Geol.*, *126*(1), 43–64.
- Lécuyer, C., G. Gruau, C. R. Anhaeusser, and S. Fourcade (1994), The origin of fluids and the effect of metamorphism on the primary chemical compositions of Barberton komatiites: New evidence from geochemical (REE) and isotopic (Nd, O, H, $^{39}\text{Ar}/^{40}\text{Ar}$) data, *Geochim. Cosmochim. Acta*, *58*(2), 969–984.
- Ludwig, K. R. (2003), ISOPLOT 3.00. A geochronological toolkit for Microsoft Excel, Berkeley Geochronol. Cent. Spec. Publ., *4*, 70 pp.
- Maier, W. D., S. J. Barnes, I. H. Campbell, M. L. Fiorentini, P. Peltonen, S. J. Barnes, and R. H. Smithies (2009), Progressive mixing of meteoritic veneer into the early Earth's deep mantle, *Nature*, *460*(7255), 620–623.
- Marks, N. E., L. E. Borg, I. D. Hutcheon, B. Jacobsen, and R. N. Clayton (2014), Samarium-neodymium chronology and rubidium-strontium systematics of an Allende calcium-aluminum-rich inclusion with implications for ^{146}Sm half-life, *Earth Planet. Sci. Lett.*, *405*, 15–24.
- McDonough, W. F. (2004), Compositional model for the Earth's core, in *Treatise on Geochemistry*, vol. 2, pp. 547–568, Elsevier, Amsterdam.
- Mertzman, S. A. (2000), K-Ar results from the southern Oregon-northern California Cascade range, *Oregon Geol.*, *62*(4), 99–122.
- Morgan, J. W., G. A. Wanderless, R. K. Petrie, and A. J. Irving (1981), Composition of the earth's upper mantle, I. Siderophile trace elements in ultramafic nodules, *Tectonophysics*, *75*(1–2), 47–67.
- Nesbitt, R. W., S. S. Sun, and A. C. Purvis (1979), Komatiites: Geochemistry and genesis, *Can. Mineral.*, *17*(2), 165–186.
- Newsom, H. E., and H. Palme (1984), The depletion of siderophile elements in the Earth's mantle: New evidence from molybdenum and tungsten, *Earth Planet. Sci. Lett.*, *69*(2), 354–364.
- Newsom, H. E., K. W. W. Sims, P. D. Noll, W. L. Jaeger, S. A. Maehr, and T. B. Beserra (1996), The depletion of tungsten in the bulk silicate Earth: Constraints on core formation, *Geochim. Cosmochim. Acta*, *60*(5), 1155–1169.
- Nimmo, F., and T. Kleine (2015), Early differentiation and core formation: Processes and timescales, in *The Early Earth*, edited by J. Badro and M. J. Walter, pp. 83–102, John Wiley, Hoboken, N. J.
- O'Neil, J., R. W. Carlson, D. Francis, and R. K. Stevenson (2008), Neodymium-142 evidence for Hadean mafic crust, *Science*, *321*(5897), 1828–1831.
- O'Neill, H. S. C., and H. Palme (2008), Collisional erosion and the non-chondritic composition of the terrestrial planets, *Philos. Trans. R. Soc. A*, *366*(1883), 4205–4238.
- Puchtel, I. S., and M. Humayun (2005), Highly siderophile element geochemistry of ^{187}Os -enriched 2.8-Ga Kostomuksha komatiites, Baltic Shield, *Geochim. Cosmochim. Acta*, *69*(6), 1607–1618.
- Puchtel, I. S., A. W. Hofmann, K. Mezger, K. P. Jochum, A. A. Shchipansky, and A. V. Samsonov (1998), Oceanic plateau model for continental crustal growth in the Archaean: A case study from the Kostomuksha greenstone belt, NW Baltic Shield, *Earth Planet. Sci. Lett.*, *155*(1–2), 57–74.
- Puchtel, I. S., M. Humayun, A. Campbell, R. Sproule, and C. M. Lesher (2004), Platinum group element geochemistry of komatiites from the Alexo and Pyke Hill areas, Ontario, Canada, *Geochim. Cosmochim. Acta*, *68*(6), 1361–1383.
- Puchtel, I. S., A. D. Brandon, M. Humayun, and R. J. Walker (2005), Evidence for the early differentiation of the core from Pt-Re-Os isotope systematics of 2.8-Ga komatiites, *Earth Planet. Sci. Lett.*, *237*(1–2), 118–134.
- Puchtel, I. S., M. Humayun, and R. J. Walker (2007), Os-Pb-Nd isotope and highly siderophile and lithophile trace element systematics of komatiitic rocks from the Volotsk suite, SE Baltic Shield, *Precambrian Res.*, *158*(1–2), 119–137.
- Puchtel, I. S., R. J. Walker, C. R. Anhaeusser, and G. Gruau (2009), Re-Os isotope systematics and HSE abundances of the 3.5 Ga Schapenburg komatiites, South Africa: Hydrous melting or prolonged survival of primordial heterogeneities in the mantle?, *Chem. Geol.*, *262*(3–4), 355–369.
- Puchtel, I. S., J. Blichert-Toft, M. Touboul, R. J. Walker, G. Byerly, E. G. Nisbet, and C. R. Anhaeusser (2013), Insights into early Earth from Barberton komatiites: Evidence from lithophile isotope and trace element systematics, *Geochim. Cosmochim. Acta*, *108*, 63–90.
- Puchtel, I. S., R. J. Walker, M. Touboul, E. G. Nisbet, and G. R. Byerly (2014), Insights into Early Earth from the Pt-Re-Os isotope and Highly Siderophile Element abundance systematics of Barberton komatiites, *Geochim. Cosmochim. Acta*, *125*, 394–413.

- Puchtel, I. S., M. Touboul, J. Blichert-Toft, R. J. Walker, A. D. Brandon, R. W. Nicklas, V. S. Kulikov, and A. V. Samsonov (2016), Lithophile and siderophile element systematics of the Earth's mantle at the Archean-Proterozoic boundary: Evidence from 2.4 Ga komatiites, *Geochim. Cosmochim. Acta*, *180*, 227–255.
- Pyke, D. R., A. J. Naldrett, and O. R. Eckstrand (1973), Archean ultramafic flows in Munro Township, Ontario, *Geol. Soc. Am. Bull.*, *84*(3), 955–978.
- Righter, K., and C. K. Shearer (2003), Magmatic fractionation of Hf and W: Constraints on the timing of core formation and differentiation in the Moon and Mars, *Geochim. Cosmochim. Acta*, *67*(13), 2497–2507.
- Rizo, H., M. Boyet, J. Blichert-Toft, and M. Rosing (2011), Combined Nd and Hf isotope evidence for deep-seated source of Isua lavas, *Earth Planet. Sci. Lett.*, *312*(3–4), 267–279.
- Rizo, H., M. Boyet, J. Blichert-Toft, J. O'Neil, M. T. Rosing, and J.-L. Paquette (2012), The elusive Hadean enriched reservoir revealed by ^{142}Nd deficits in Isua Archean rocks, *Nature*, *491*(7422), 96–100.
- Rizo, H., M. Boyet, J. Blichert-Toft, and M. T. Rosing (2013), Early mantle dynamics inferred from ^{142}Nd variations in Archean rocks from southwest Greenland, *Earth Planet. Sci. Lett.*, *377*–378, 324–335.
- Rizo, H., R. J. Walker, R. W. Carlson, M. Touboul, M. F. Horan, I. S. Puchtel, M. Boyet, and M. T. Rosing (2016), Early Earth differentiation investigated through ^{142}Nd , ^{182}W , and highly siderophile element abundances in samples from Isua, Greenland, *Geochim. Cosmochim. Acta*, *175*, 319–336.
- Roth, A. S. G., B. Bourdon, S. J. Mojzsis, M. Touboul, P. Sprung, M. Guitreau, and J. Blichert-Toft (2013), Inherited ^{142}Nd anomalies in Eoarchean protoliths, *Earth Planet. Sci. Lett.*, *361*, 50–57.
- Roth, A. S. G., B. Bourdon, S. J. Mojzsis, J. F. Rudge, M. Guitreau, and J. Blichert-Toft (2014), Combined $^{147,146}\text{Sm}$ – $^{143,142}\text{Nd}$ constraints on the longevity and residence time of early terrestrial crust, *Geochem. Geophys. Geosyst.*, *15*, 2329–2345, doi:10.1002/2014GC005313.
- Rubie, D. C., D. J. Frost, U. Mann, Y. Asahara, F. Nimmo, K. Tsuno, P. Kegler, A. Holzheid, and H. Palme (2011), Heterogeneous accretion, composition and core-mantle differentiation of the Earth, *Earth Planet. Sci. Lett.*, *301*(1–2), 31–42.
- Salters, V. J. M., and J. Longhi (1999), Trace element partitioning during the initial stages of melting beneath mid-ocean ridges, *Earth Planet. Sci. Lett.*, *166*(1–2), 15–30.
- Scherer, E., C. Münker, and K. Mezger (2001), Calibration of the lutetium-hafnium clock, *Science*, *293*(5530), 683–687.
- Scherstén, A., T. Elliott, C. Hawkesworth, and M. Norman (2004), Tungsten isotope evidence that mantle plumes contain no contribution from the Earth's core, *Nature*, *427*(6971), 234–237.
- Shirey, S. B., and R. J. Walker (1998), The Re-Os isotope system in cosmochemistry and high-temperature geochemistry, *Annu. Rev. Earth Planet. Sci.*, *26*, 423–500.
- Smoliar, M. I., R. J. Walker, and J. W. Morgan (1996), Re-Os ages of Group IIA, IIIA, IVA, and IVB iron meteorites, *Science*, *271*(5762), 1099–1102.
- Söderlund, U., J. P. Patchett, J. D. Vervoort, and C. E. Isachsen (2004), The ^{176}Lu decay constant determined by Lu-Hf and U-Pb isotope systematics of Precambrian mafic intrusions, *Earth Planet. Sci. Lett.*, *219*(3–4), 311–324.
- Touboul, M., and R. J. Walker (2012), High precision tungsten isotope measurement by thermal ionization mass spectrometry, *Int. J. Mass Spectrom.*, *309*, 109–117.
- Touboul, M., I. S. Puchtel, and R. J. Walker (2012), ^{182}W Evidence for long-term preservation of early mantle differentiation products, *Science*, *335*, 1065–1069.
- Touboul, M., J. Liu, J. O'Neil, I. S. Puchtel, and R. J. Walker (2014), New insights into the Hadean Mantle revealed by ^{182}W and highly siderophile element abundances of supracrustal rocks from the Nuvvuagittuq Greenstone Belt, Quebec, Canada, *Chem. Geol.*, *383*, 63–75.
- Touboul, M., I. S. Puchtel, and R. J. Walker (2015), Tungsten isotopic evidence for disproportional late accretion to the Earth and Moon, *Nature*, *520*(7548), 530–533.
- Vervoort, J. D., and J. Blichert-Toft (1999), Evolution of the depleted mantle: Hf isotope evidence from juvenile rocks through time, *Geochim. Cosmochim. Acta*, *63*(3–4), 533–556.
- Viljoen, M. J., and R. P. Viljoen (1969), The geology and geochemistry of the Lower Ultramafic Unit of the Onverwacht Group and a proposed new class of igneous rocks, *Geol. Soc. S. Afr. Spec. Publ.*, *2*, 55–86.
- Viljoen, M. J., R. P. Viljoen, H. S. Smith, and A. J. Erlank (1983), Geological, textural and geochemical features of komatiitic flows from the Komati Formation, *Geol. Soc. S. Afr. Spec. Publ.*, *9*, 1–20.
- Willbold, M., T. Elliott, and S. Moorbath (2011), The tungsten isotopic composition of the Earth's mantle before the terminal bombardment, *Nature*, *477*(7363), 195–198.
- Willbold, M., S. J. Mojzsis, H. W. Chen, and T. Elliott (2015), Tungsten isotope composition of the Acasta Gneiss Complex, *Earth Planet. Sci. Lett.*, *419*, 168–177.
- Yin, Q.-Z., S. B. Jacobsen, K. Yamashita, J. Blichert-Toft, P. Télouk, and F. Albarède (2002), A short time scale for terrestrial planet formation from Hf-W chronometry of meteorites, *Nature*, *418*, 949–952.